

Article

Late Cretaceous Activity Record of the Guansan Fault—Insights from Zircon U-Pb and Apatite Fission-Track Thermochronology

Ruxin Ding ^{1,2,3,*}, Weihao Chen ¹, Cleber Soares ⁴, Weisheng Hou ^{1,*}, Zilong Li ¹, Yangshijia Li ¹, Rongli Huang ¹ and Heping Zou ¹

- ¹ Guangdong Provincial Key Laboratory of Geodynamics and Geohazards, School of Earth Sciences and Engineer, Sun Yat-sen University, Zhuhai 519000, China
² Guangdong Provincial Key Laboratory of Geological Process and Mineral Resource Exploration, Guangzhou 510275, China
³ Southern Marine Science and Engineering Guangdong Laboratory (Zhuhai), Zhuhai 519000, China
⁴ ChronusCamp Research-Thermochronology Analysis LTD, Itapira 13975-088, Brazil
* Correspondence: dingrux@mail.sysu.edu.cn (R.D.); houwsh@mail.sysu.edu.cn (W.H.)

Abstract: The timing of fault activity is a concern for geologists. This study used zircon U-Pb and apatite fission-track dating of fault breccia to determine the upper and lower limits for the time of faulting. The Guansan fault in South China was taken as an example, and zircon U-Pb and apatite fission-track thermochronology were applied to the surrounding rock and fault breccia. The surrounding rock and fault breccia demonstrated 74.9–91.8 Ma and 73.9–93.5 Ma zircon U-Pb dates, respectively, indicating that the breccia formed after 73.9 Ma. They also demonstrated 71.6 ± 7.3 Ma and 85.9 ± 8.2 – 65.5 ± 6.5 Ma fission-track dates, implying that the fault breccia samples likely formed before ~ 70 Ma. Their thermal histories were highly consistent: both showed rapid cooling during 70–65 Ma and slow cooling during 65–0 Ma, implying that the fault was likely still active during 70–65 Ma, resulting in the rapid exhumation.

Keywords: zircon U-Pb; apatite fission-track; Guansan fault; thermochronology



Citation: Ding, R.; Chen, W.; Soares, C.; Hou, W.; Li, Z.; Li, Y.; Huang, R.; Zou, H. Late Cretaceous Activity Record of the Guansan

Fault—Insights from Zircon U-Pb and Apatite Fission-Track

Thermochronology. *Minerals* **2022**, *12*, 1163. <https://doi.org/10.3390/min12091163>

Academic Editors: Carlos Alberto Tello Sáenz and Jim Lee

Received: 27 June 2022

Accepted: 8 September 2022

Published: 14 September 2022

Publisher's Note: MDPI stays neutral with regard to jurisdictional claims in published maps and institutional affiliations.



Copyright: © 2022 by the authors. Licensee MDPI, Basel, Switzerland. This article is an open access article distributed under the terms and conditions of the Creative Commons Attribution (CC BY) license (<https://creativecommons.org/licenses/by/4.0/>).

1. Introduction

The timing of fault activity is usually determined according to the stratigraphic units cut by the fault, and there are several methods that can be used to date the fault rocks directly, such as Ar-Ar dating of mylonites (e.g., [1,2]) and electron spin resonance dating of fault gouges (e.g., [3,4]). Since the end of the last century, low-temperature thermochronology has created new possibilities for obtaining the timing of fault activity; e.g., using apatite fission-track (AFT) dating to date fault gouges (e.g., [5–9]), cataclasite (e.g., [10,11]) and mylonite (e.g., [9,12]) or using horizontal or vertical sections to estimate fault history (e.g., [13–15]). Although these methods can be used to directly date fault rocks or to constrain the surrounding rock evolution on both sides of the fault, they also have certain disadvantages; for example, it is difficult to determine the time span of fault activity using a single dating method, and a large number of samples are needed to compare the date variations across the fault.

This paper proposes to constrain the age of fault activity by using both zircon U-Pb and apatite fission-tracking to date the formation of fault breccia. This approach is suitable for studies of the faults with few outcrops; e.g., hidden faults passing through a city. We studied the Guansan fault to illustrate this approach. The Guansan fault is a deep and hidden fault [16] across from the urban centre of Guangzhou, a large city of more than 10 million people, that has influences on urban construction and earthquake hazards [17]. Dating the fault activity helps us to understand the evolution of the fault.

2. Geological Setting and Sampling

The Guansan fault, with a depth of 30 km [18,19], is the middle section of the Gaoyao–Huilai fault, which is one of the longest EW-trending faults in the South China Block. The Gaoyao–Huilai fault zone (Figure 1a) is located in southern China, near the South China Sea. It is about 200 km long and 10–60 km wide [16]. It determines the flow direction of the rivers and the topography of the Pearl River drainage, which is one of the biggest drainage systems supplying the northern South China Sea (Figure 1a). The fault formed during the Trassic and was again active during the Jurassic–Cretaceous with granite intrusion and volcanic overflow along the fault; e.g., basalt and trachyte (64–57 Ma) [16].

The Guansan fault and Shougouling faults are both located in the middle section of the Gaoyao–Huilai fault zone and are the two branches of the fault zone (Figure 1a). Studies have mainly focused on the Shougouling fault. Zou et al. obtained a $^{40}\text{Ar}/^{39}\text{Ar}$ plateau date of 172.27 Ma from the mylonite [20]. Zhu et al. obtained AFT dates of 36.2 ± 0.9 Ma, 29.9 ± 4.4 Ma and 27.1 ± 4.3 Ma for fault gouges [6]. Quaternary fault activity has also been documented [6,20,21]. Unlike the Shougouling fault, which is exposed between the Cretaceous strata and intrusive rocks, the Guansan fault is mostly hidden under the Quaternary strata. Therefore, study of the Guansan fault is still limited to the Quaternary strata [21–23]. This study provides new evidence of the pre-Quaternary history of Guansan fault.

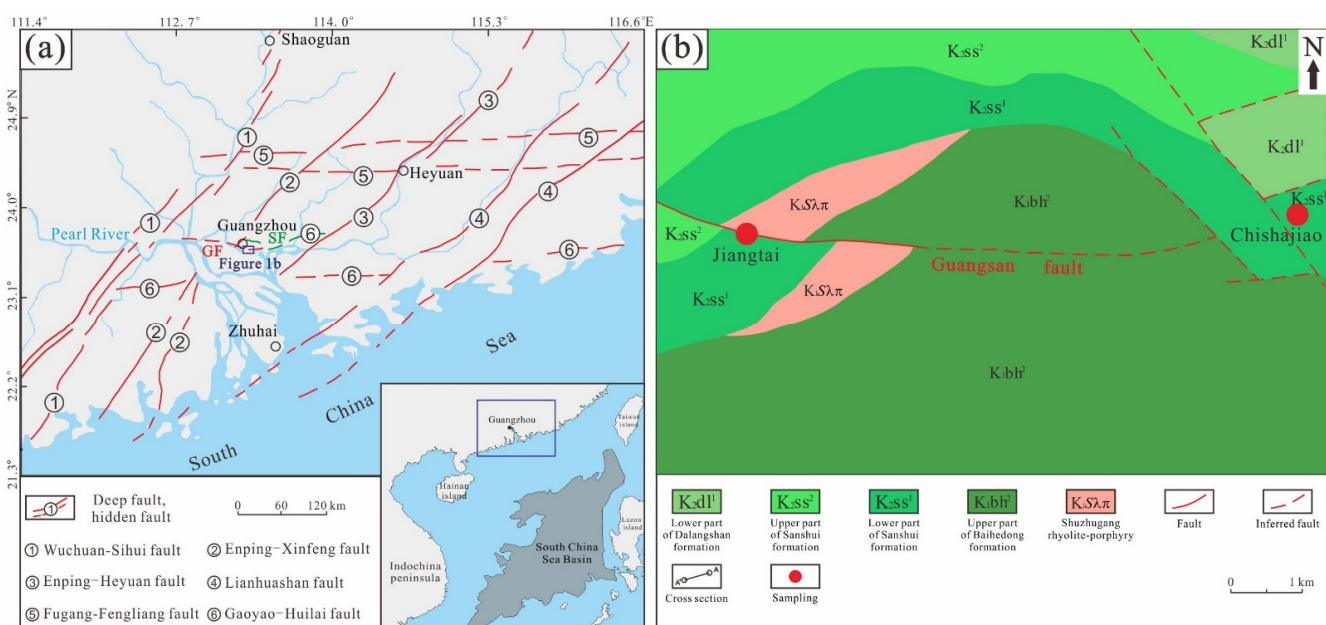


Figure 1. Geological map of the study area. (a) Location map of Gaoyao–Huilai fault in Guangdong province, China (modified from [24,25]). Figure 1b indicated to geological map of the study area. GF: Guansan fault; SF: Shougouling fault. (b) Geological map of the study area (modified from [26]).

The strata exposed in the study area include Cretaceous and Quaternary strata (Figure 1b). The Cretaceous strata are composed of the Baihedong formation, Sanshui formation and Dalangshan formation, from bottom to up [27]. The temporal boundaries between the formations are 93 and 80 Ma, respectively [28]. The Baihedong formation comprises siltstone and mudstone with thin interlayers of limestone and gypsum, the Sanshui formation comprises red sandstone and conglomerate with thin interlayers of gypsum and the Dalangshan formation comprises sandstone and mudstone [27–29]. Both the Sanshui formation and Dalangshan formation contain granitic conglomerates, and those of the Dalangshan formation are coarser than those of the Sanshui formation [29]. The Baihedong formation, Sanshui formation and Shuzhugang rock body (mainly composed of rhyolite porphyry) are cut by the Guansan fault and form a sinistral strike-slip fault.

Seven samples were collected in Guangzhou city along the fault zone: four samples (#1, #2, #3, #4) from the deep subway excavation (samples #2 and #4 were located perpendicular to the direction of the fault and were up to tens of meters wide, while samples #1 and #3 were located on the fault plane; see Appendix A), two samples from drill rock cores (MKZ2-A90, TTL-23) at Jiangtai Road subway station and the final sample (#7) from drill rock core nearby Chishajiao subway station. Samples #2, #4 and TTL-23 were rhyolite porphyry (country rock), samples #1, #3 and MKZ2-A90 were fault breccia (fault rock) and sample #7 was conglomerate (country rock) from the Sanshui formation. Photos of the samples are shown in Appendix B. Zircon U-Pb dating was conducted on all samples and AFT dating on four samples (#1, #3, MKZ2-A90 and TTL-23).

3. Analytical Methods

Zircon and apatite were separated by crushing, sieving and magnetic and heavy-liquid separation and then handpicked under a binocular microscope. Then, the zircon and apatite grains were mounted in epoxy resin and polished to expose internal surfaces.

The zircon grains were photographed using a JSM-IT100 scanning electron microscope (JEOL Ltd., Tokyo, Japan) coupled to a Gatan MiniCL cathodoluminescence (CL) spectroscope (Gatan, Inc., Pleasanton, CA, USA). Zircon U-Pb dating was performed using an Agilent 7900 inductively coupled plasma–mass spectrometer coupled to a GeoLas HD 193 nm laser ablation system at SampleSolution Analytical Technology Co., Ltd in Wuhan, China. Argon was used as the make-up gas and mixed with the carrier gas Helium before use in the plasma–mass spectrometer. The spot size and frequency of the laser were set to 32 μm and 5 Hz, respectively. Zircon 91500, GJ-1, Plesovice and glass NIST610 were used as external standards. The software packages ICPMSDataCal [30] and Isoplot v3.06 [31] were used to perform the quantitative calibration for U-Pb dating and to plot concordia diagrams, respectively.

Apatite grains were etched with 5.5 M HNO_3 for 20 s at 21 °C. Then, direct U determination was performed using an Agilent 7800 inductively coupled plasma–mass spectrometer coupled (Agilent, Yokogawa, Japan) to a New Wave UP 213 nm laser ablation system at Isotope Geology Laboratory of ChronusCamp in São Paulo, Brazil. A mixture of argon (950 mL/min), helium (440 mL/min) and hydrogen (4.5 mL/min) was used as the carrier gas for the plasma–mass spectrometer. The laser spot size was set to 40 μm and the frequency to 5 Hz. The Mud Tank and Durango apatites were used as the standard samples [32,33]. The AFT dates of the grains were calculated from the spontaneous fission-track density and the U concentration. Then, the confined fission-track lengths were measured under an optical microscope. The software Low-T Thermo (V5.0) [34] was used to perform the thermal history modelling.

4. Analytical Results

4.1. Zircon U-Pb Dating

A total of 25 spots on the zircon grains were dated for each sample. CL images of the analysed zircon grains are illustrated in Appendix C, and all spots were located at the edges of the zircons, which meant that the dates were representative of the latest crystallographic regrowths. All the zircons were euhedral or subhedral, except for a few zircons from sample #7, which were rounded. The grain sizes mainly ranged from 70 to 200 μm . They exhibited clear oscillatory zoning. All the analyses (Appendix D) indicated Th/U ratios > 0.1, most of them > 0.4, indicating that all the zircons were of magmatic origin. The zircon dating U-Pb concordia diagrams are illustrated in Figure 2. The $^{207}\text{Pb}/^{206}\text{Pb}$ ages of the zircons (>1000 Ma) and $^{206}\text{Pb}/^{238}\text{U}$ ages of the remaining zircons were used for the discussion.

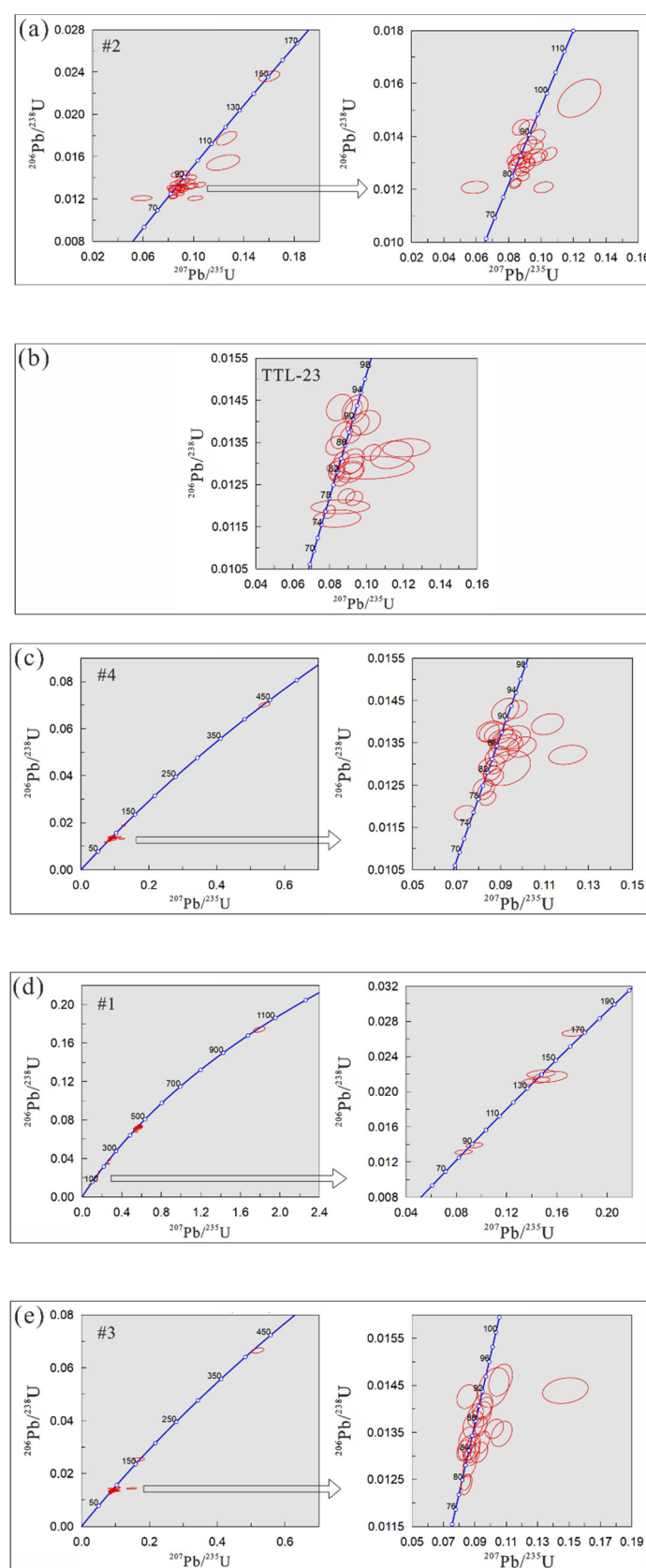


Figure 2. Cont.

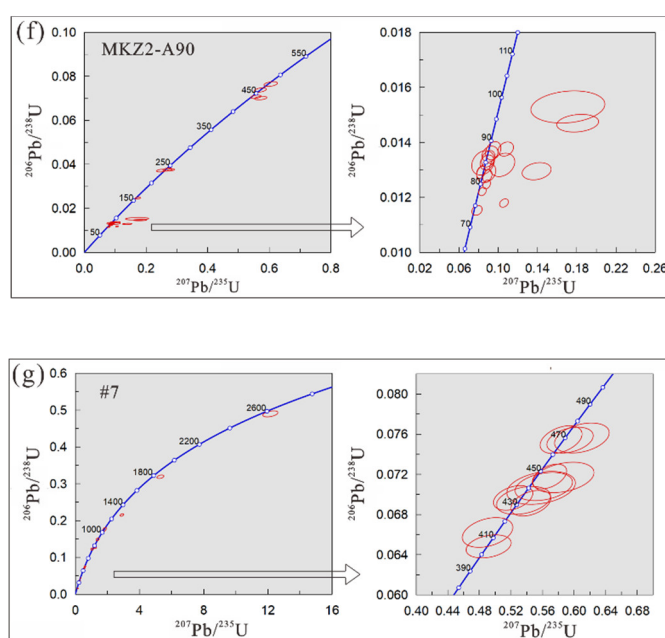


Figure 2. Zircon dating U-Pb concordia diagrams for this study. (a) sample #2, (b) sample TTL-23 and (c) sample #4 are country rock. (d) sample #1, (e) sample #3, (f) sample MKZ2-A90 are fault rock and (g) sample #7.

The zircon grains of sample #2 were 70–150 μm long. Among the 20 spot analyses with concordances $\geq 90\%$, the dates of 18 data points were concentrated in the late Cretaceous (91.8–78.2 Ma). The dates of two were early Cretaceous (113 ± 2.7 Ma and 150 ± 2.1 Ma).

Most zircon grains of sample #4 were 140–200 μm long. Among the 22 spot analyses with concordances $\geq 90\%$, the dates of 20 data points were concentrated in the late Cretaceous (91.5–75.9 Ma). The dates of two were early Cretaceous (120 ± 1.2 Ma) and one was early Paleozoic (437 ± 4.1 Ma).

The zircon grains of sample TTL-23 were mostly 130–200 μm long. The dates of 20 data points with concordances $\geq 90\%$ were concentrated in the late Cretaceous (91.7–74.9 Ma).

The zircon grains of sample #1 were mostly 100–200 μm . Among the 25 spot analyses with concordances $\geq 90\%$, the dates of two data points were late Cretaceous (88.2 ± 1.2 Ma and 82.1 ± 1.0 Ma), five were early Cretaceous (169–135 Ma) and two were Triassic (218 \pm 1.9 Ma and 243 ± 2.8 Ma), while 15 of the data points were concentrated in the early Paleozoic (422–462 Ma) with a weighted mean of 449.8 ± 3.8 Ma ($N = 14$, MSWD = 2.7). Only one data point was dated to the Proterozoic (1050 ± 46 Ma).

The zircon grains of sample #3 were mostly 150–200 μm . Among the 22 spot analyses with concordances $\geq 90\%$, 20 points were concentrated in the late Cretaceous (93.5–79.4 Ma). The other two were Jurassic (161 ± 2.7 Ma) and early Paleozoic (415 ± 3.8 Ma).

The zircon grains of sample MKZ2-A90 were mostly 90~200 μm . Among the 19 spot analyses with concordances $\geq 90\%$, 11 data points were concentrated in the late Cretaceous (87.7–73.9 Ma). The date of one was Jurassic (157 ± 1.4 Ma), the dates of three points were Triassic (238–235 Ma) and the dates of four points were early Paleozoic (475–437 Ma).

The zircon grains of sample #7 were mostly 90–200 μm . Among the 23 spot analyses with concordances $\geq 90\%$, the date of one was early Cretaceous (103 ± 1.5 Ma). The dates of 2 were Triassic (233 ± 2.7 Ma and 235 ± 2.4 Ma) and the dates of 12 were concentrated in the early Paleozoic (405–470 Ma) with a weighted mean of 438.5 ± 6.2 Ma ($N = 7$, MSWD = 1.5). The dates of seven were Proterozoic (747–2637 Ma).

4.2. AFT Analysis Results

The AFT results for four samples (TTL-23, #1, #3 and MKZ2-A90) are summarized in Table 1, and the detailed results are listed in Appendix E. The AFT date of the rhyolite porphyry sample TTL-23 was 71.6 ± 7.3 Ma and the AFT dates of the fault breccia samples (#1, #3 and MKZ2-A90) were 65.5 ± 6.5 Ma, 69.3 ± 6.3 Ma and 85.9 ± 8.2 Ma, respectively.

Table 1. The AFT results for this study.

Sample	Depth (m)	N (Grains)	N _s (Tracks)	Rho (s) $\times 10^6$	Rho (Zeta) $\times 10^5$	Zeta (mMS) $\times 10^3$	U _{UNK} ($\mu\text{g/g}$)	Pooled Age (Ma)	Central Age (Ma)	Minimum Age (Ma)	p (χ^2)	Mean Length (μm)	n (Tracks)
TTL-23	41.8–41.9	40	169	0.26	1.65	1.772	9.06	51.5 ± 4.2	71.6 ± 7.3	52.1 ± 13.1	0.01	14.92 ± 0.84	98
#1	~24	37	106	0.82	1.65	1.772	2.25	57.9 ± 5.8	65.5 ± 6.5	65.4 ± 6.5	0.93	14.93 ± 0.93	35
#3	~26	40	127	0.19	1.65	1.772	5.65	61.9 ± 5.8	69.3 ± 6.3	69.5 ± 6.8	0.95	14.77 ± 0.97	108
MKZ2-A90	28	40	145	0.23	1.65	1.822	5.26	70.0 ± 6.8	85.9 ± 8.2	73.1 ± 8.0	0.49	14.82 ± 0.87	47

Note: All the errors are 1σ . n: number of confined tracks.

Although sample TTL-23 had the largest dispersion (Figure 3) and the lowest $p(\chi^2)$ -value (Table 1), the overdispersion was ignored because the sample was rhyolite porphyry. All the other samples had lower dispersions (Figure 3) and passed the χ^2 -test ($p(\chi^2) > 5\%$, Table 1), implying that these three samples most likely had only one single date population. The mean track lengths of all samples ranged from $14.77 \pm 0.97 \mu\text{m}$ to $14.93 \pm 0.93 \mu\text{m}$ (Table 1), and the length distributions of all samples were unimodal, with a peak at $\sim 15 \mu\text{m}$ (Figure 4), indicating fast cooling histories since the length standards were comparable to most age standards and the standard deviations were $<1 \mu\text{m}$.

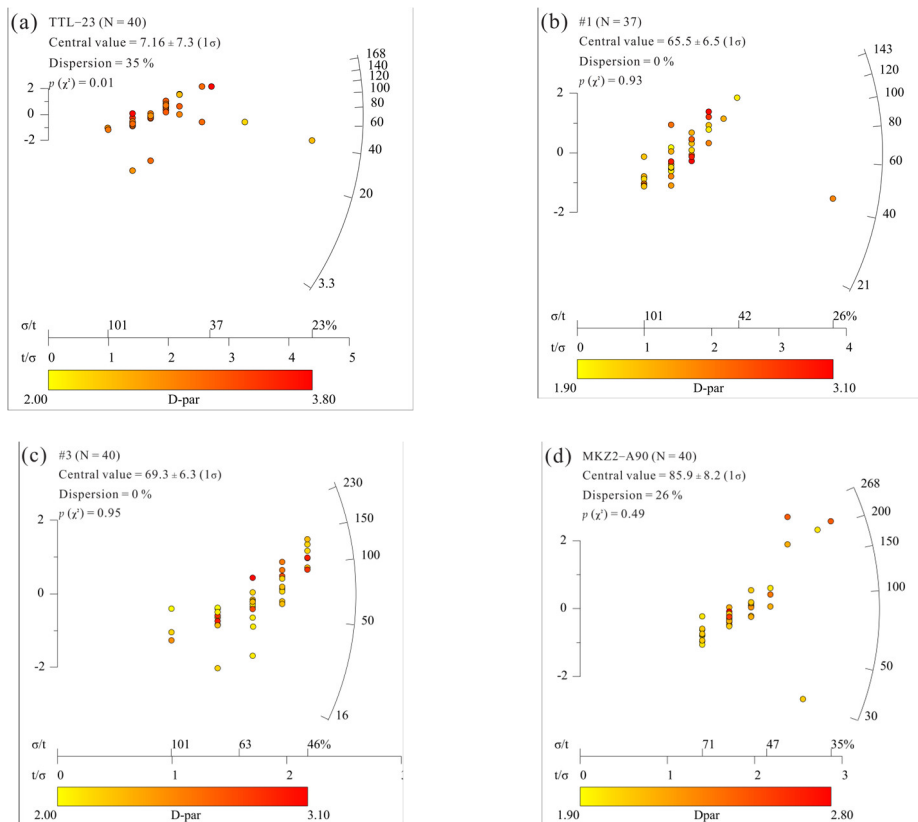


Figure 3. Radial plots of the single-grain AFT ages made using RadialPlotter [35]. (a) sample TTL-23 is country rock. (b) sample #1, (c) sample #3 and (d) sample MKZ2-90 are fault rock.

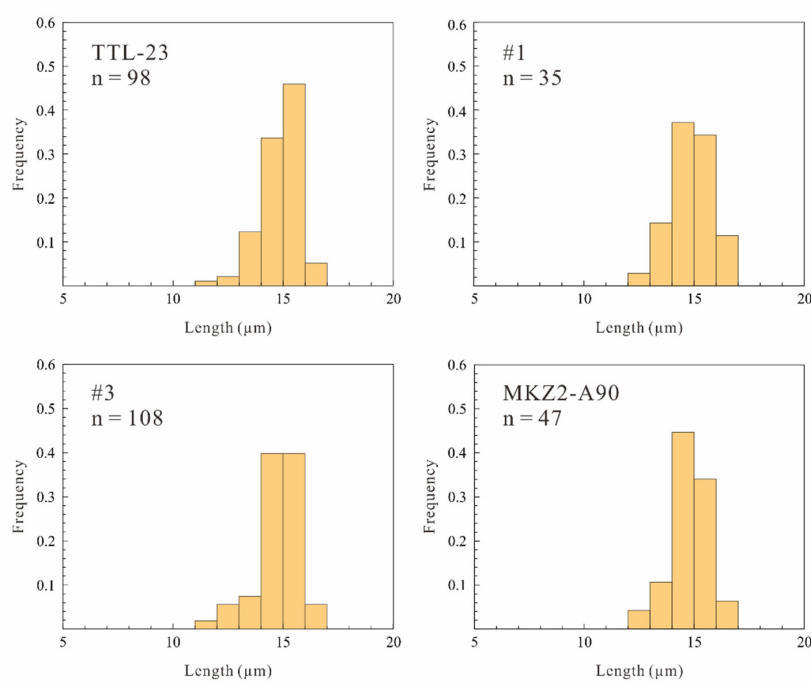


Figure 4. Confined track length distributions.

The thermal history modelling was conducted for samples TTL-23 and #3 as they had sufficient confined tracks ($n = 98$ and 108 , respectively). D_{par} was not used for compositional correction. For the thermal history modelling, we used the following parameters and models: the surface temperatures at sea level were set to 20°C ; the fanning curvilinear fit annealing model [36] was used as the AFT annealing model for c -axis projected track lengths; the c -axis projected confined track-length distribution was used for the Kolmogorov-Smirnov test; and the initial c -axis projected track length was set to $16.3\text{ }\mu\text{m}$. The overall fit was determined by the minimum of two probabilities (age and length). The results are shown in Figure 5. The mean thermal histories (MTHs) within the 50% confidence intervals (i.e., goodness-of-fit (GOF) ≥ 0.5) were used as the final thermal history modelling result. The results indicated that the thermal histories of samples TTL-23 and #3 showed relatively rapid cooling from 70 to 65 Ma and slow cooling from 65 to 0 Ma . Their results are remarkably consistent.

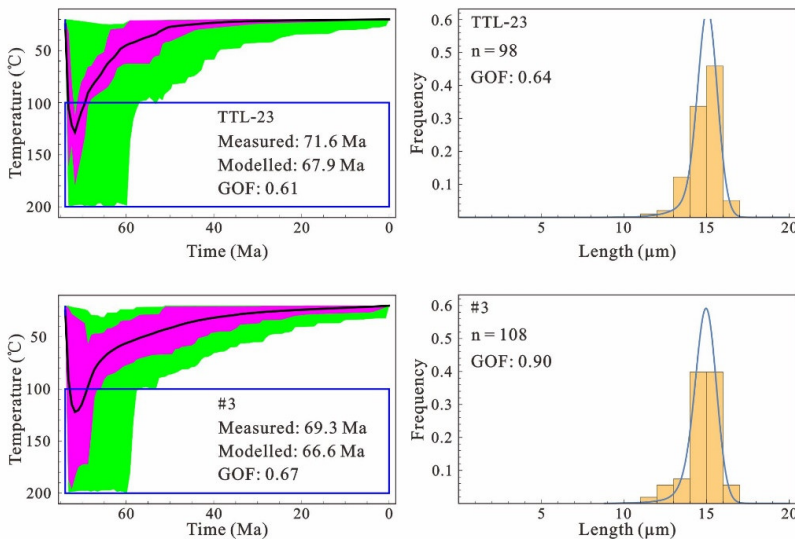


Figure 5. Thermal history models of samples TTL-23 and #3. The Low-T Thermo computer code [34]

was used for the modelling. The 1,000,000 t-T paths were randomly generated using the Monte Carlo method. The blue indicates the substantial range used to search for reheating. The mean of all good t-T paths (i.e., goodness-of-fit (GOF) ≥ 0.5) was calculated and assumed to be the most likely t-T path of the sample. The blue boxes were defined to constrain the reheated model during the modeling moderation. The black solid lines represent the mean thermal histories (MTHs) used as the final thermal history modelling result. The magenta areas define the envelopes of good fit (GOF ≥ 0.5). The green areas define the envelopes of acceptable fit (GOF ≥ 0.05).

5. Discussion

The zircon U-Pb dates of the rhyolite porphyry samples from country rock were concentrated in the late Cretaceous. In contrast, the zircon U-Pb dates of the sedimentary samples from country rock ranged from early Cretaceous, Triassic and early Paleozoic to Proterozoic. The zircon U-Pb dates of the fault-zone samples were also dispersed, ranging from late Cretaceous, late Jurassic–early Cretaceous and early Paleozoic to Proterozoic. This implies that the source rock of the fault breccia samples was most likely rhyolite porphyry and sedimentary rock.

The late Cretaceous zircon U-Pb dates of the three rhyolite porphyry samples were concentrated in the range from 91.8 to 74.9 Ma, and the late Cretaceous zircon U-Pb dates of the three fault breccias were concentrated in the range from 93.5 to 73.9 Ma. Combining these two groups, it can be inferred that there was multiple-stage magmatic activity or an extended period of volcanic activity in the late Cretaceous from 93.5 to 73.9 Ma. Therefore, the entire zircon U-Pb dataset was used to obtain a maximum age for the faulting since the faulting occurred after the deposition of the rhyolite porphyry; i.e., the faulting occurred after 73.9 Ma.

The AFT results, which indicated similar AFT dates (around 70 Ma), unimodal distribution of AFT confined lengths (Figure 4) and high χ^2 values for AFT grain dates (Table 1), implied that the three fault breccia samples likely underwent complete annealing with the rhyolite porphyry around 70 Ma. This also implied that the fault breccia samples likely formed before \sim 70 Ma. Both friction and hydrothermal infilling are possible reason for this reset, but further research is needed.

Based on the reheating model, the thermal history modelling results of samples TTL-23 and #3 showed rapid cooling during 70–65 Ma and slow cooling during 65–0 Ma. The cooling trends of both samples were highly consistent. One possible reason is that the rock from samples TTL-23 and #3 underwent the same cooling history after the forming of the fault breccia. Another possible reason is that the rock from sample #3 was cut during periods of uncertainty, as most of the zircon U-Pb dates from sample #3 were late Cretaceous, and rhyolite porphyry was most likely the main material. In either case, the implication is that the fault was likely still active during 70–65 Ma and causing rapid exhumation.

The Dalangshan formation around the Guanshan fault includes granitic gravels coarser than those of the Sanshui formation [29]. The Dalangshan formation is roughly contemporaneous with the faulting, which implies that the fault zone possibly provided coarse material for the Dalangshan formation. Rapid exhumation also occurred during \sim 60–80 Ma along the continental margin of the South China Block [37–39], suggesting that both the faulting and exhumation were probably driven by extensional collapse of the continental margin of the South China Block after the Yanshan orogeny [16,20].

6. Conclusions

We present a method for dating faulting. It involves comparing the zircon U-Pb dating of both surrounding rock and fault breccia to determine whether the breccia originates from the surrounding rock, providing an upper limit for the time of faulting. The apatite fission-track dates of the surrounding rock and fault breccia provide a lower limit for the time of faulting.

When applied to the Guansan fault in South China, the results revealed that the surrounding rock had zircon U-Pb dates of 91.8~74.9 Ma and the fault breccia dates of 93.5~73.9 Ma. The two kinds of rocks had similar AFT dates of around 70 Ma and underwent rapid cooling during 70–65 Ma. This implies that faulting along Guansan fault likely occurred during ~73–65 Ma.

Author Contributions: Conceptualization: R.D.; methodology: R.D.; resources: W.H. and H.Z.; funding acquisition: R.D., W.H. and H.Z.; investigation: W.C., C.S., Z.L. and R.D.; formal analysis: R.D. and W.C.; validation: R.D. and W.H.; writing—original draft preparation: R.D.; writing—review and editing, R.D., Y.L., R.H., W.C., C.S. and H.Z.; project administration: R.D. All authors have read and agreed to the published version of the manuscript.

Funding: This study was jointly supported by the National Natural Science Foundation of China (nos. 42072229; 41972049; 52078507; 41972302 and 41977231), the Science and Technology Program of Guangzhou (nos. 202002030184 and 202102080395), the Guangdong Natural Science Foundation (no. 2021A1515011658), the Special Fund for Basic Scientific Research of Central Colleges, Chang'an University (no. 300102260502), and the Innovation Group Project of Southern Marine Science and Engineering Guangdong Laboratory (Zhuhai) (no. 311021003).

Data Availability Statement: Not applicable.

Conflicts of Interest: The authors declare no conflict of interest regarding the publication of this paper.

Appendix A

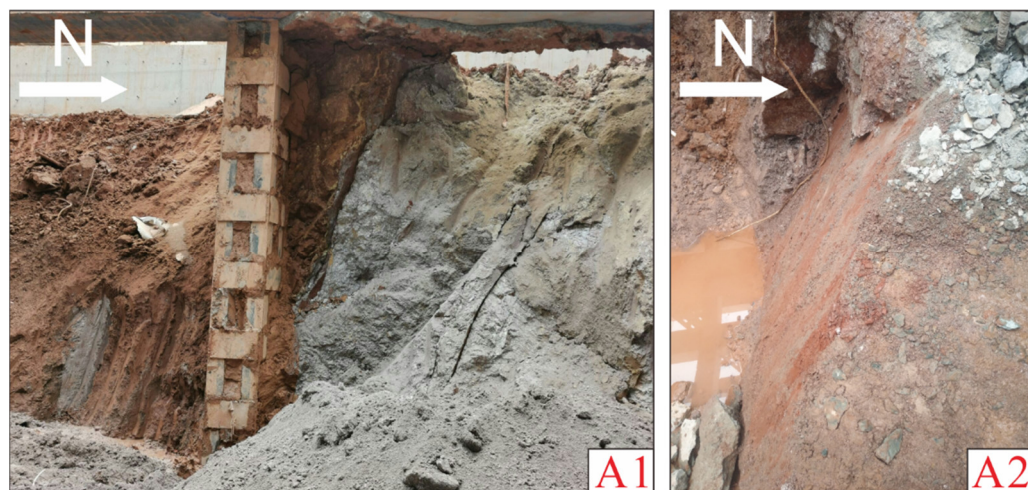


Figure A1. Photos of sample locations in the deep subway excavation at Jiangtai Road subway station. (A1) Cretaceous sediments on the left and volcanic rocks on the right; (A2) fault plane (the plane dips to the south with a dip angle of 52°).

Appendix B

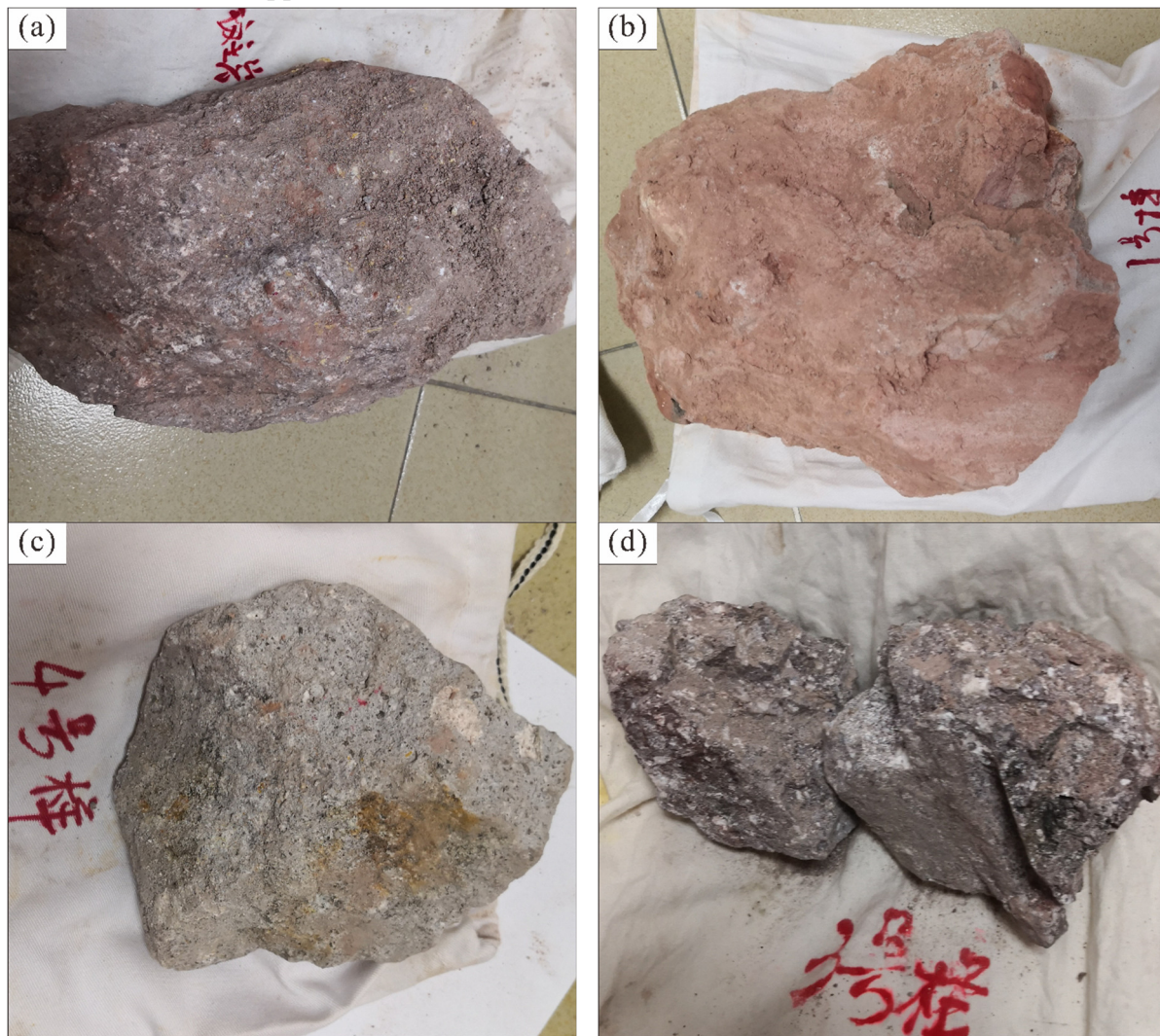


Figure A2. *Cont.*

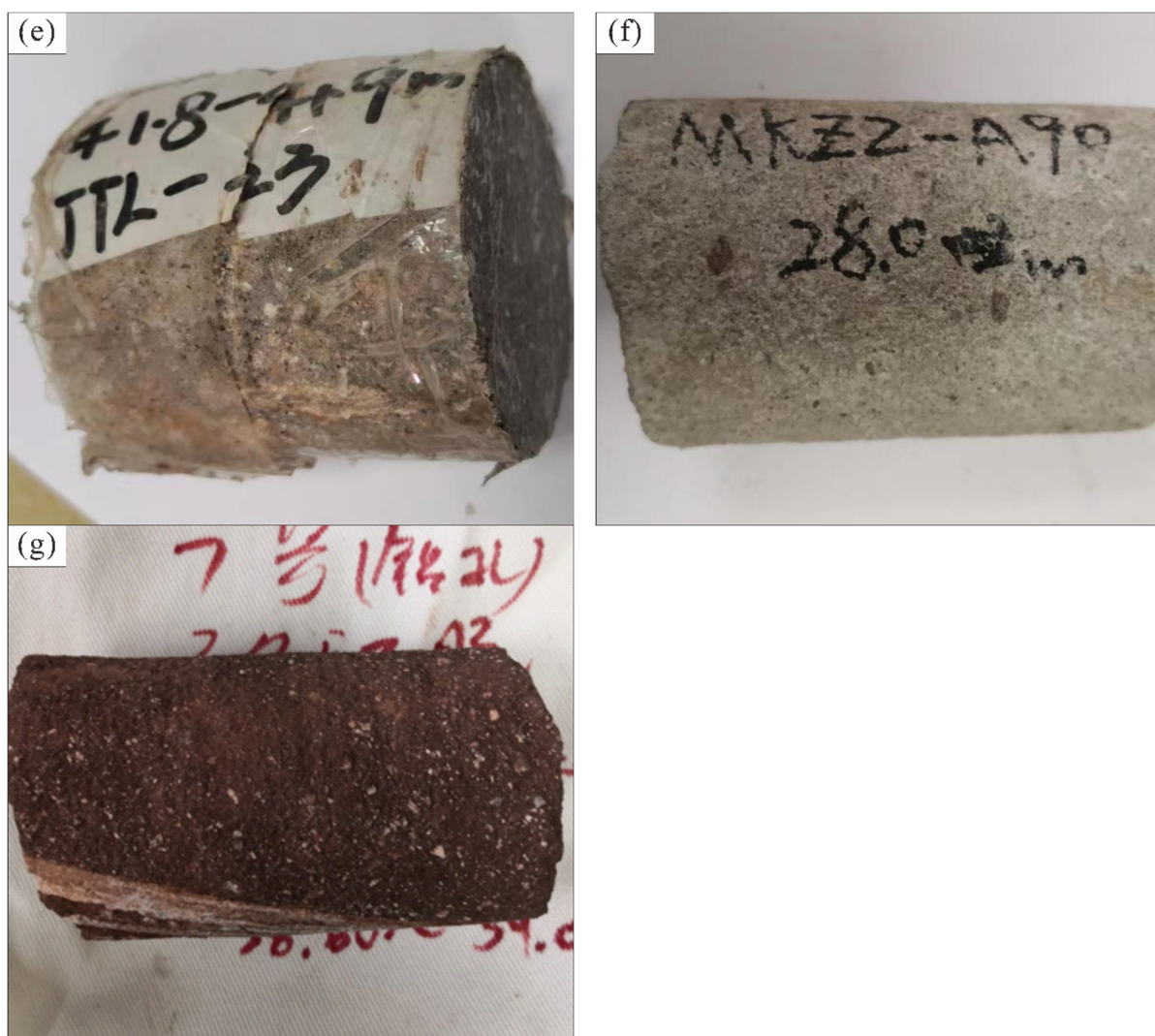


Figure A2. Photos of samples in this study. (a) sample #2; (b) sample #1; (c) sample #4; (d) sample #3; (e) sample TTL-23; (f) sample MKZ2-A90; (g) sample #7.

Appendix C

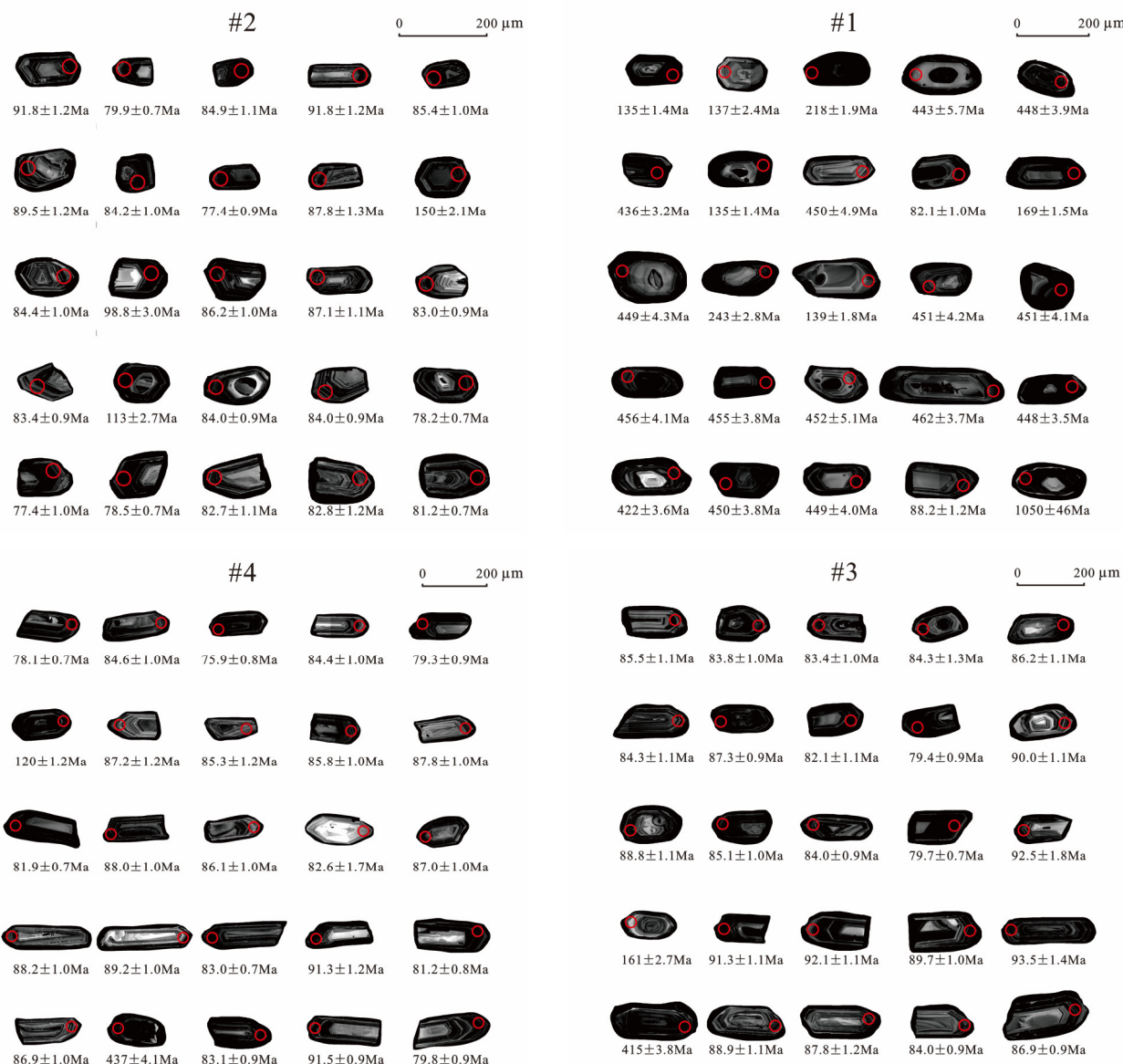


Figure A3. Cont.



Figure A3. Zircon CL images. The red circle in all figures indicate the spot position of Zircon U-Pb dating.

Appendix D

Table A1. Zircon U-Pb dating results analysed in this study.

Sample	Pb	Th	U	Th/U	$^{207}\text{Pb}/^{206}\text{Pb}$		$^{207}\text{Pb}/^{235}\text{U}$		$^{206}\text{Pb}/^{238}\text{U}$		$^{207}\text{Pb}/^{206}\text{U}$		$^{207}\text{Pb}/^{235}\text{U}$		$^{206}\text{Pb}/^{238}\text{U}$	
	ppm	ppm	ppm	Ratio	Ratio	1 σ	Ratio	1 σ	Ratio	1 σ	Date (Ma)	1 σ (Ma)	Date (Ma)	1 σ (Ma)	Date (Ma)	1 σ (Ma)
#2—rhyolite porphyry																
#2-01	46.0	1950	2636	0.74	0.0466	0.0018	0.0918	0.0035	0.0143	0.0002	27.9	93	89.2	3	91.8	1
#2-02	99.0	3982	6448	0.62	0.0517	0.0015	0.0890	0.0025	0.0125	0.0001	333	67	86.6	2	79.9	1
#2-03	73.9	2130	4096	0.52	0.0521	0.0026	0.0963	0.0049	0.0133	0.0002	300	113	93.4	5	84.9	1
#2-04	48.6	2079	2723	0.76	0.0444	0.0018	0.0875	0.0034	0.0143	0.0002	-	-	85.1	3	91.8	1
#2-05	67.4	2038	4251	0.48	0.0573	0.0018	0.1050	0.0031	0.0133	0.0002	502	69	101	3	85.4	1
#2-06	46.8	1764	2754	0.64	0.0505	0.0017	0.0974	0.0034	0.0140	0.0002	217	47	94.4	3	89.5	1
#2-07	68.8	2277	4389	0.52	0.0536	0.0018	0.0974	0.0033	0.0131	0.0002	354	74	94.4	3	84.2	1
#2-08	123.5	4288	6862	0.62	0.0611	0.0024	0.1015	0.0040	0.0121	0.0001	643	86	98.1	4	77.4	1
#2-09	38.5	1245	2391	0.52	0.0483	0.0020	0.0914	0.0039	0.0137	0.0002	122	98	88.8	4	87.8	1
#2-10	54.24	329	2139	0.15	0.0491	0.0016	0.1602	0.0055	0.0236	0.0003	150	81	151	5	150	2
#2-11	30.12	1173	1834	0.64	0.0490	0.0021	0.0885	0.0037	0.0132	0.0002	146	106	86.1	3	84.4	1
#2-12	49.2	1684	3045	0.55	0.0549	0.0024	0.1236	0.0087	0.0154	0.0005	406	98	118	8	98.8	3
#2-13	37.0	1385	2239	0.62	0.0473	0.0022	0.0879	0.0042	0.0135	0.0002	64.9	104	85.5	4	86.2	1
#2-14	26.0	1254	1483	0.85	0.0505	0.0026	0.0942	0.0047	0.0136	0.0002	217	119	91.4	4	87.1	1
#2-15	39.98	1211	2593	0.47	0.0479	0.0020	0.0852	0.0036	0.0130	0.0001	100	91	83.0	3	83.0	1
#2-16	41.0	1376	2598	0.53	0.0506	0.0020	0.0905	0.0036	0.0130	0.0001	233	97	87.9	3	83.4	1
#2-17	56.36	895	2941	0.30	0.0507	0.0016	0.1263	0.0053	0.0177	0.0004	233	74	121	5	113	3
#2-18	39.9	1551	2437	0.64	0.0469	0.0020	0.0843	0.0035	0.0131	0.0001	42.7	100	82.2	3	84.0	1
#2-19	38.4	1182	2414	0.49	0.0479	0.0019	0.0864	0.0033	0.0131	0.0001	94.5	89	84.2	3	84.0	1
#2-20	81.1	2274	5592	0.41	0.0500	0.0014	0.0841	0.0023	0.0122	0.0001	198	65	82.0	2	78.2	1
#2-21	91.0	2704	5006	0.54	0.0359	0.0033	0.0590	0.0054	0.0121	0.0002	-	-	58.2	5	77.4	1
#2-22	96.0	1776	6900	0.26	0.0497	0.0012	0.0844	0.0021	0.0123	0.0001	183	57	82.3	2	78.5	1
#2-23	53.0	2258	3264	0.69	0.0514	0.0017	0.0915	0.0031	0.0129	0.0002	261	78	88.9	3	82.7	1
#2-24	39.3	1416	2485	0.57	0.0488	0.0025	0.0865	0.0044	0.0129	0.0002	139	122	84.2	4	82.8	1
#2-25	55.7	2521	3439	0.73	0.0504	0.0016	0.0883	0.0028	0.0127	0.0001	213	74	85.9	3	81.2	1

Table A1. *Cont.*

Sample	Pb	Th	U	Th/U	$^{207}\text{Pb}/^{206}\text{Pb}$		$^{207}\text{Pb}/^{235}\text{U}$		$^{206}\text{Pb}/^{238}\text{U}$		$^{207}\text{Pb}/^{206}\text{U}$		$^{207}\text{Pb}/^{235}\text{U}$		$^{206}\text{Pb}/^{238}\text{U}$	
	ppm	ppm	ppm	Ratio	Ratio	1 σ	Ratio	1 σ	Ratio	1 σ	Date (Ma)	1 σ (Ma)	Date (Ma)	1 σ (Ma)	Date (Ma)	1 σ (Ma)
#4—rhyolite porphyry																
#4-01	24.04	860	1691	0.51	0.0498	0.0013	0.0842	0.0024	0.0122	0.0001	187	63	82.1	2	78.1	1
#4-02	9.37	433	556	0.78	0.0661	0.0031	0.1206	0.0057	0.0132	0.0001	809	98	116	5	84.6	1
#4-03	33.6	1837	1943	0.95	0.0453	0.0019	0.0736	0.0030	0.0118	0.0001	-	-	72.1	3	75.9	1
#4-04	11.86	635	703	0.90	0.0489	0.0021	0.0885	0.0036	0.0132	0.0002	139	102	86.1	3	84.4	1
#4-05	23.91	877	1679	0.52	0.0487	0.0015	0.0834	0.0026	0.0124	0.0001	200	75	81.4	2	79.3	1
#4-06	24.61	353	1235	0.29	0.0481	0.0014	0.1257	0.0038	0.0188	0.0002	106	69	120	3	120	1
#4-07	8.33	426	462	0.92	0.0513	0.0028	0.0961	0.0050	0.0136	0.0002	254	128	93.2	5	87.2	1
#4-08	8.71	292	543	0.54	0.0504	0.0027	0.0915	0.0045	0.0133	0.0002	217	122	88.9	4	85.3	1
#4-09	8.39	363	519	0.70	0.0542	0.0024	0.0996	0.0044	0.0134	0.0002	389	102	96.4	4	85.8	1
#4-10	6.66	232	416	0.56	0.0473	0.0024	0.0892	0.0043	0.0137	0.0002	64.9	124	86.8	4	87.8	1
#4-11	24.37	809	1647	0.49	0.0489	0.0016	0.0861	0.0026	0.0128	0.0001	143	76	83.8	2	81.9	1
#4-12	16.89	622	1063	0.59	0.0447	0.0016	0.0848	0.0030	0.0137	0.0002	-	-	82.7	3	88.0	1
#4-13	6.31	297	373	0.79	0.0501	0.0027	0.0930	0.0047	0.0134	0.0002	211	121	90.3	4	86.1	1
#4-14	2.96	229	155	1.48	0.0533	0.0050	0.0930	0.0070	0.0129	0.0003	343	208	90.3	7	82.6	2
#4-15	10.94	512	657	0.78	0.0483	0.0023	0.0907	0.0043	0.0136	0.0002	122	98	88.2	4	87.0	1
#4-16	10.50	416	646	0.64	0.0454	0.0022	0.0854	0.0042	0.0138	0.0002	-	-	83.2	4	88.2	1
#4-17	9.54	404	544	0.74	0.0579	0.0025	0.1113	0.0048	0.0139	0.0002	528	96	107	4	89.2	1
#4-18	17.97	763	1146	0.67	0.0472	0.0016	0.0842	0.0028	0.0130	0.0001	61.2	81	82.0	3	83.0	1
#4-19	12.28	404	753	0.54	0.0474	0.0022	0.0921	0.0041	0.0143	0.0002	77.9	98	89.5	4	91.3	1
#4-20	23.71	706	1632	0.43	0.0497	0.0015	0.0872	0.0027	0.0127	0.0001	189	73	84.9	3	81.2	1
#4-21	8.92	380	536	0.71	0.0502	0.0026	0.0928	0.0045	0.0136	0.0002	211	119	90.1	4	86.9	1
#4-22	94.4	407	1211	0.34	0.0557	0.0010	0.5414	0.0109	0.0702	0.0007	439	41	439	7	437	4
#4-23	17.59	621	1158	0.54	0.0485	0.0016	0.0874	0.0029	0.0130	0.0001	124	71	85.1	3	83.1	1
#4-24	16.05	437	979	0.45	0.0493	0.0017	0.0972	0.0033	0.0143	0.0001	161	81	94.2	3	91.5	1
#4-25	17.89	659	1221	0.54	0.0475	0.0016	0.0819	0.0029	0.0125	0.0001	76.0	78	79.9	3	79.8	1

Table A1. *Cont.*

Sample	Pb	Th	U	Th/U	$^{207}\text{Pb}/^{206}\text{Pb}$		$^{207}\text{Pb}/^{235}\text{U}$		$^{206}\text{Pb}/^{238}\text{U}$		$^{207}\text{Pb}/^{206}\text{U}$		$^{207}\text{Pb}/^{235}\text{U}$		$^{206}\text{Pb}/^{238}\text{U}$	
	ppm	ppm	ppm	Ratio	Ratio	1 σ	Ratio	1 σ	Ratio	1 σ	Date (Ma)	1 σ (Ma)	Date (Ma)	1 σ (Ma)	Date (Ma)	1 σ (Ma)
TTL-23—rhyolite porphyry																
TTL-23-01	38.1	793	2227	0.36	0.0498	0.0027	0.0910	0.0052	0.0128	0.0001	183	128	88.5	5	82.2	1
TTL-23-02	19.9	630	643	0.98	0.0520	0.0082	0.1021	0.0156	0.0129	0.0002	287	326	98.7	14	82.6	1
TTL-23-03	8.12	414	424	0.98	0.0484	0.0026	0.0937	0.0046	0.0143	0.0002	117	126	91.0	4	91.4	1
TTL-23-04	23.08	767	1508	0.51	0.0476	0.0015	0.0864	0.0027	0.0131	0.0001	83.4	74	84.1	3	83.9	1
TTL-23-05	12.21	472	740	0.64	0.0491	0.0020	0.0952	0.0041	0.0139	0.0002	150	101	92.3	4	89.1	1
TTL-23-06	6.84	253	409	0.62	0.0522	0.0030	0.0996	0.0053	0.0140	0.0002	295	127	96.4	5	89.4	1
TTL-23-07	8.40	429	471	0.91	0.0439	0.0026	0.0853	0.0046	0.0143	0.0002	-	-	83.1	4	91.7	1
TTL-23-08	24.13	1172	1414	0.83	0.0558	0.0017	0.1028	0.0033	0.0133	0.0001	456	73	99.4	3	84.9	1
TTL-23-09	18.76	607	1269	0.48	0.0495	0.0017	0.0865	0.0029	0.0126	0.0001	169	84	84.2	3	81.0	1
TTL-23-10	15.64	527	944	0.56	0.0471	0.0016	0.0927	0.0032	0.0143	0.0002	57.5	74	90.0	3	91.2	1
TTL-23-11	28.58	600	1804	0.33	0.0593	0.0034	0.1136	0.0076	0.0132	0.0002	589	124	109	7	84.6	1
TTL-23-12	17.04	1033	951	1.09	0.0518	0.0019	0.0926	0.0035	0.0130	0.0002	276	90	89.9	3	83.2	1
TTL-23-13	9.65	379	607	0.62	0.0514	0.0026	0.0912	0.0047	0.0128	0.0002	261	117	88.6	4	81.9	1
TTL-23-14	36.5	1032	2234	0.46	0.0523	0.0017	0.0890	0.0030	0.0122	0.0001	298	69	86.6	3	78.4	1
TTL-23-15	37.1	1151	1978	0.58	0.0507	0.0049	0.0840	0.0085	0.0117	0.0001	233	202	81.9	8	74.9	1
TTL-23-16	14.51	483	901	0.54	0.0450	0.0019	0.0833	0.0036	0.0134	0.0001	-	-	81.2	3	86.0	1
TTL-23-17	13.93	442	847	0.52	0.0483	0.0019	0.0913	0.0036	0.0137	0.0001	122	93	88.7	3	87.6	1
TTL-23-18	39.6	1020	1773	0.58	0.0504	0.0063	0.0858	0.0105	0.0120	0.0001	213	267	83.6	10	76.7	1
TTL-23-19	26.23	813	1763	0.46	0.0552	0.0017	0.0933	0.0030	0.0122	0.0001	420	69	90.6	3	78.0	1
TTL-23-20	29.51	780	2133	0.37	0.0487	0.0014	0.0797	0.0022	0.0119	0.0001	132	67	77.9	2	75.9	1
TTL-23-21	12.32	474	773	0.61	0.0463	0.0020	0.0865	0.0038	0.0137	0.0002	13.1	109	84.3	4	87.5	1
TTL-23-22	6.44	241	402	0.60	0.0516	0.0026	0.0919	0.0046	0.0130	0.0002	333	121	89.3	4	83.6	1
TTL-23-23	21.44	749	1401	0.53	0.0470	0.0016	0.0839	0.0030	0.0129	0.0002	55.7	72	81.9	3	82.5	1
TTL-23-24	15.96	708	898	0.79	0.0644	0.0041	0.1216	0.0085	0.0134	0.0001	755	133	117	8	85.6	1
TTL-23-25	23.83	649	1590	0.41	0.0477	0.0013	0.0843	0.0025	0.0128	0.0001	87.1	67	82.2	2	81.7	1

Table A1. *Cont.*

Sample	Pb	Th	U	Th/U	$^{207}\text{Pb}/^{206}\text{Pb}$		$^{207}\text{Pb}/^{235}\text{U}$		$^{206}\text{Pb}/^{238}\text{U}$		$^{207}\text{Pb}/^{206}\text{U}$		$^{207}\text{Pb}/^{235}\text{U}$		$^{206}\text{Pb}/^{238}\text{U}$	
	ppm	ppm	ppm	Ratio	Ratio	1 σ	Ratio	1 σ	Ratio	1 σ	Date (Ma)	1 σ (Ma)	Date (Ma)	1 σ (Ma)	Date (Ma)	1 σ (Ma)
#1—fault breccia																
#1-01	100.7	1282	4216	0.30	0.0503	0.0014	0.1474	0.0042	0.0212	0.0002	209	65	140	4	135	1
#1-02	15.69	382	594	0.64	0.0511	0.0030	0.1494	0.0082	0.0214	0.0004	256	142	141	7	137	2
#1-03	188.3	1738	4838	0.36	0.0559	0.0012	0.2662	0.0062	0.0344	0.0003	456	48	240	5	218	2
#1-04	25.71	130	310	0.42	0.0574	0.0029	0.5595	0.0278	0.0712	0.0009	506	109	451	18	443	6
#1-05	98.3	621	1142	0.54	0.0563	0.0014	0.5602	0.0146	0.0720	0.0006	465	57	452	10	448	4
#1-06	162.1	914	1961	0.47	0.0556	0.0012	0.5391	0.0119	0.0701	0.0005	439	48	438	8	436	3
#1-07	92.1	1411	3858	0.37	0.0481	0.0013	0.1396	0.0039	0.0211	0.0002	102	67	133	4	135	1
#1-08	49.0	331	561	0.59	0.0565	0.0020	0.5593	0.0194	0.0722	0.0008	472	78	451	13	450	5
#1-09	85.8	3349	4834	0.69	0.0451	0.0029	0.0768	0.0045	0.0128	0.0002	-	-	75.1	4	82.1	1
#1-10	55.5	844	1749	0.48	0.0477	0.0017	0.1748	0.0061	0.0266	0.0002	83.4	81	164	5	169	2
#1-11	88.4	496	1035	0.48	0.0568	0.0016	0.5659	0.0162	0.0722	0.0007	483	63	455	11	449	4
#1-12	45.3	506	987	0.51	0.0515	0.0018	0.2744	0.0100	0.0384	0.0004	265	77	246	8	243	3
#1-13	25.90	502	998	0.50	0.0484	0.0025	0.1442	0.0070	0.0218	0.0003	120	115	137	6	139	2
#1-14	84.9	529	973	0.54	0.0581	0.0015	0.5816	0.0148	0.0725	0.0007	600	56	465	10	451	4
#1-15	149.2	745	1780	0.42	0.0571	0.0013	0.5709	0.0127	0.0725	0.0007	494	44	459	8	451	4
#1-16	75.7	306	911	0.34	0.0579	0.0017	0.5836	0.0163	0.0732	0.0007	524	63	467	10	456	4
#1-17	161.3	507	1995	0.25	0.0578	0.0014	0.5845	0.0142	0.0732	0.0006	520	47	467	9	455	4
#1-18	30.17	201	346	0.58	0.0583	0.0025	0.5778	0.0237	0.0727	0.0008	539	94	463	15	452	5
#1-19	108.2	502	1267	0.40	0.0564	0.0014	0.5792	0.0148	0.0743	0.0006	478	57	464	10	462	4
#1-20	259.3	1134	3165	0.36	0.0573	0.0011	0.5706	0.0110	0.0719	0.0006	506	43	458	7	448	4
#1-21	228.0	1053	2948	0.36	0.0581	0.0011	0.5442	0.0109	0.0677	0.0006	600	38	441	7	422	4
#1-22	92.93	205	1194	0.17	0.0560	0.0014	0.5583	0.0139	0.0722	0.0006	454	57	450	9	450	4
#1-23	209.6	555	2677	0.21	0.0565	0.0012	0.5636	0.0122	0.0722	0.0007	472	42	454	8	449	4
#1-24	30.93	962	1939	0.50	0.0495	0.0023	0.0935	0.0042	0.0138	0.0002	172	107	90.7	4	88.2	1
#1-25	289.1	204	1533	0.13	0.0743	0.0015	1.7904	0.0399	0.1740	0.0018	1050	46	1042	15	1034	10

Table A1. *Cont.*

Sample	Pb	Th	U	Th/U	$^{207}\text{Pb}/^{206}\text{Pb}$		$^{207}\text{Pb}/^{235}\text{U}$		$^{206}\text{Pb}/^{238}\text{U}$		$^{207}\text{Pb}/^{206}\text{U}$		$^{207}\text{Pb}/^{235}\text{U}$		$^{206}\text{Pb}/^{238}\text{U}$	
	ppm	ppm	ppm	Ratio	Ratio	1 σ	Ratio	1 σ	Ratio	1 σ	Date (Ma)	1 σ (Ma)	Date (Ma)	1 σ (Ma)	Date (Ma)	1 σ (Ma)
#3—fault breccia																
#3-01	42.6	1654	2626	0.63	0.0464	0.0019	0.0852	0.0036	0.0133	0.0002	16.8	106	83.0	3	85.5	1
#3-02	39.8	2345	2217	1.06	0.0512	0.0020	0.0928	0.0036	0.0131	0.0001	250	92	90.1	3	83.8	1
#3-03	49.0	2928	2841	1.03	0.0491	0.0019	0.0879	0.0033	0.0130	0.0001	154	89	85.6	3	83.4	1
#3-04	55.6	2106	3661	0.58	0.0488	0.0016	0.0886	0.0032	0.0132	0.0002	139	78	86.2	3	84.3	1
#3-05	29.70	1033	1817	0.57	0.0581	0.0024	0.1071	0.0044	0.0135	0.0002	532	89	103	4	86.2	1
#3-06	20.44	900	1264	0.71	0.0480	0.0027	0.0863	0.0045	0.0132	0.0002	98.2	135	84.0	4	84.3	1
#3-07	124.1	4631	7470	0.62	0.0500	0.0013	0.0940	0.0025	0.0136	0.0001	195	63	91.2	2	87.3	1
#3-08	89.6	3159	6200	0.51	0.0490	0.0014	0.0867	0.0029	0.0128	0.0002	146	69	84.5	3	82.1	1
#3-09	117.1	2593	8698	0.30	0.0494	0.0012	0.0847	0.0023	0.0124	0.0001	165	62	82.5	2	79.4	1
#3-10	29.7	1474	1661	0.89	0.0494	0.0022	0.0950	0.0042	0.0141	0.0002	169	136	92.1	4	90.0	1
#3-11	47.6	1903	2881	0.66	0.0475	0.0018	0.0904	0.0033	0.0139	0.0002	76.0	85	87.9	3	88.8	1
#3-12	69.3	2731	4341	0.63	0.0514	0.0015	0.0947	0.0030	0.0133	0.0002	261	69	91.9	3	85.1	1
#3-13	62.2	2212	4051	0.55	0.0478	0.0014	0.0865	0.0027	0.0131	0.0001	100	75	84.2	2	84.0	1
#3-14	104.5	2375	7645	0.31	0.0489	0.0012	0.0842	0.0021	0.0124	0.0001	146	49	82.1	2	79.7	1
#3-15	4.42	176	257	0.68	0.0524	0.0038	0.1019	0.0066	0.0145	0.0003	302	167	98.5	6	92.5	2
#3-16	3.84	60.6	133	0.45	0.0495	0.0035	0.1690	0.0112	0.0253	0.0004	169	159	159	10	161	3
#3-17	8.17	337	474	0.71	0.0432	0.0022	0.0850	0.0042	0.0143	0.0002	-	-	82.8	4	91.3	1
#3-18	18.57	654	1046	0.62	0.0719	0.0039	0.1477	0.0096	0.0144	0.0002	983	111	140	8	92.1	1
#3-19	14.87	433	941	0.46	0.0500	0.0017	0.0963	0.0033	0.0140	0.0002	195	75	93.4	3	89.7	1
#3-20	13.23	396	807	0.49	0.0520	0.0021	0.1064	0.0050	0.0146	0.0002	283	93	103	5	93.5	1
#3-21	49.3	279	655	0.43	0.0564	0.0012	0.5195	0.0122	0.0665	0.0006	478	51	425	8	415	4
#3-22	11.86	494	702	0.70	0.0493	0.0021	0.0944	0.0040	0.0139	0.0002	165	96	91.6	4	88.9	1
#3-23	5.94	265	354	0.75	0.0480	0.0025	0.0891	0.0043	0.0137	0.0002	102	119	86.6	4	87.5	1
#3-24	12.74	657	775	0.85	0.0461	0.0017	0.0832	0.0031	0.0131	0.0001	400	-300	81.2	3	84.0	1
#3-25	11.67	366	738	0.50	0.0547	0.0021	0.1025	0.0039	0.0136	0.0001	398	81	99.0	4	86.9	1

Table A1. *Cont.*

Sample	Pb	Th	U	Th/U	$^{207}\text{Pb}/^{206}\text{Pb}$		$^{207}\text{Pb}/^{235}\text{U}$		$^{206}\text{Pb}/^{238}\text{U}$		$^{207}\text{Pb}/^{206}\text{U}$		$^{207}\text{Pb}/^{235}\text{U}$		$^{206}\text{Pb}/^{238}\text{U}$	
	ppm	ppm	ppm	Ratio	Ratio	1 σ	Ratio	1 σ	Ratio	1 σ	Date (Ma)	1 σ (Ma)	Date (Ma)	1 σ (Ma)	Date (Ma)	1 σ (Ma)
MKZ2-A90—fault breccia																
MKZ2-A90-01	6.92	345	408	0.85	0.0506	0.0029	0.0949	0.0052	0.0137	0.0002	220	135	92.1	5	87.7	1
MKZ2-A90-02	2.31	140	132	1.06	0.0484	0.0053	0.0846	0.0077	0.0133	0.0003	117	237	82.5	7	84.9	2
MKZ2-A90-03	7.43	371	416	0.89	0.0571	0.0030	0.1077	0.0052	0.0138	0.0002	494	115	104	5	88.1	1
MKZ2-A90-04	28.34	818	2025	0.40	0.0496	0.0015	0.0839	0.0026	0.0122	0.0001	189	75	81.8	2	78.3	1
MKZ2-A90-05	5.13	263	294	0.90	0.0782	0.0056	0.1392	0.0098	0.0130	0.0002	1151	138	132	9	83.0	1
MKZ2-A90-06	2.59	198	132	1.49	0.0605	0.0060	0.1042	0.0084	0.0132	0.0003	633	221	101	8	84.4	2
MKZ2-A90-07	7.03	196	465	0.42	0.0491	0.0027	0.0886	0.0046	0.0133	0.0002	154	128	86.2	4	85.0	1
MKZ2-A90-08	48.20	423	1139	0.37	0.0543	0.0015	0.2812	0.0076	0.0375	0.0003	383	68	252	6	237	2
MKZ2-A90-09	2.48	132	123	1.07	0.0802	0.0106	0.1710	0.0249	0.0153	0.0004	1267	263	160	22	97.8	2
MKZ2-A90-10	21.5	1284	1261	1.02	0.0461	0.0016	0.0824	0.0030	0.0129	0.0001	400	-313	80.4	3	82.7	1
MKZ2-A90-11	7.10	343	420	0.82	0.0497	0.0034	0.0916	0.0053	0.0136	0.0002	189	166	89.0	5	86.9	1
MKZ2-A90-12	3.09	131	198	0.66	0.0494	0.0039	0.0878	0.0065	0.0129	0.0002	165	178	85.4	6	82.6	1
MKZ2-A90-13	37.2	1322	2274	0.58	0.0500	0.0023	0.0784	0.0035	0.0115	0.0001	195	109	76.6	3	73.9	1
MKZ2-A90-14	9.18	259	532	0.49	0.0856	0.0060	0.1810	0.0141	0.0147	0.0002	1329	136	169	12	94.1	1
MKZ2-A90-15	45.02	207	519	0.40	0.0570	0.0014	0.6049	0.0145	0.0765	0.0007	500	54	480	9	475	4
MKZ2-A90-16	6.19	275	376	0.73	0.0490	0.0027	0.0899	0.0045	0.0134	0.0002	150	128	87.4	4	85.8	1
MKZ2-A90-17	45.2	280	553	0.51	0.0589	0.0014	0.5724	0.0132	0.0701	0.0005	561	52	460	9	437	3
MKZ2-A90-18	17.35	261	379	0.69	0.0517	0.0018	0.2701	0.0099	0.0376	0.0005	276	81	243	8	238	3
MKZ2-A90-19	72.2	396	891	0.44	0.0568	0.0011	0.5566	0.0111	0.0707	0.0005	483	43	449	7	440	3
MKZ2-A90-20	18.82	287	669	0.43	0.0510	0.0019	0.1734	0.0061	0.0247	0.0002	239	83	162	5	157	1
MKZ2-A90-21	37.6	1232	2641	0.47	0.0647	0.0017	0.1059	0.0030	0.0118	0.0001	765	57	102	3	75.6	1
MKZ2-A90-22	20.91	642	1419	0.45	0.0501	0.0017	0.0890	0.0031	0.0128	0.0001	198	78	86.6	3	81.9	1
MKZ2-A90-23	25.81	812	1789	0.45	0.0514	0.0015	0.0883	0.0026	0.0125	0.0001	257	69	85.9	2	79.9	1
MKZ2-A90-24	44.50	93.2	572	0.16	0.0561	0.0012	0.5711	0.0127	0.0738	0.0006	454	48	459	8	459	4
MKZ2-A90-25	13.68	203	301	0.68	0.0487	0.0020	0.2495	0.0100	0.0372	0.0004	200	99	226	8	235	2

Table A1. *Cont.*

Sample	Pb	Th	U	Th/U	$^{207}\text{Pb}/^{206}\text{Pb}$		$^{207}\text{Pb}/^{235}\text{U}$		$^{206}\text{Pb}/^{238}\text{U}$		$^{207}\text{Pb}/^{206}\text{U}$		$^{207}\text{Pb}/^{235}\text{U}$		$^{206}\text{Pb}/^{238}\text{U}$	
	ppm	ppm	ppm	Ratio	Ratio	1σ	Ratio	1σ	Ratio	1σ	Date (Ma)	1σ (Ma)	Date (Ma)	1σ (Ma)	Date (Ma)	1σ (Ma)
#7—conglomerate																
#7-01	23.18	154	284	0.54	0.0542	0.0024	0.4903	0.0211	0.0662	0.0010	389	102	405	14	413	6
#7-02	25.71	339	563	0.60	0.0479	0.0020	0.2435	0.0098	0.0368	0.0004	98.2	96	221	8	233	3
#7-03	26.43	260	485	0.54	0.0552	0.0022	0.3326	0.0127	0.0438	0.0005	420	89	292	10	276	3
#7-04	44.4	780	954	0.82	0.0597	0.0021	0.3005	0.0095	0.0369	0.0006	591	71	267	7	234	3
#7-05	51.0	338	595	0.57	0.0539	0.0017	0.5227	0.0164	0.0697	0.0008	369	69	427	11	434	5
#7-06	102.8	66.0	166	0.40	0.1782	0.0045	12.1595	0.3109	0.4897	0.0054	2637	43	2617	24	2569	24
#7-07	60.0	138	392	0.35	0.0712	0.0023	1.2595	0.0417	0.1264	0.0015	965	65	828	19	767	9
#7-08	13.16	45.8	90.6	0.51	0.0620	0.0036	1.0510	0.0578	0.1228	0.0018	672	126	729	29	747	10
#7-09	114.7	113	460	0.25	0.0967	0.0025	2.9010	0.0736	0.2151	0.0022	1561	44	1382	19	1256	12
#7-10	27.19	160	655	0.24	0.0550	0.0022	0.2839	0.0109	0.0372	0.0004	413	91	254	9	235	2
#7-11	115.0	615	1379	0.45	0.0568	0.0014	0.5688	0.0144	0.0718	0.0008	483	56	457	9	447	5
#7-12	32.13	215	350	0.62	0.0580	0.0022	0.6099	0.0229	0.0756	0.0010	528	77	483	14	470	6
#7-13	153.7	118	407	0.29	0.1191	0.0031	5.3034	0.1402	0.3189	0.0031	1942	47	1869	23	1784	15
#7-14	26.47	142	343	0.41	0.0548	0.0022	0.4917	0.0188	0.0648	0.0008	467	95	406	13	405	5
#7-15	26.72	463	1374	0.34	0.0780	0.0028	0.1741	0.0062	0.0161	0.0002	1147	70	163	5	103	1
#7-16	34.89	168	391	0.43	0.0568	0.0019	0.5948	0.0194	0.0754	0.0008	487	79	474	12	469	5
#7-17	19.48	129	226	0.57	0.0561	0.0025	0.5358	0.0226	0.0694	0.0009	454	98	436	15	433	6
#7-18	10.77	50.3	58.4	0.86	0.0673	0.0033	1.3829	0.0654	0.1489	0.0022	850	100	882	28	895	12
#7-19	12.08	79.7	137	0.58	0.0574	0.0031	0.5581	0.0287	0.0707	0.0011	506	119	450	19	440	7
#7-20	22.31	191	244	0.78	0.0572	0.0025	0.5616	0.0240	0.0708	0.0009	498	98	453	16	441	6
#7-21	10.55	279	531	0.52	0.0557	0.0034	0.1222	0.0070	0.0160	0.0002	439	139	117	6	103	2
#7-22	68.7	285	780	0.37	0.0554	0.0016	0.5835	0.0175	0.0755	0.0009	432	65	467	11	469	5
#7-23	17.17	103	195	0.53	0.0590	0.0026	0.5865	0.0256	0.0717	0.0010	565	91	469	16	446	6
#7-24	33.0	300	352	0.85	0.0569	0.0018	0.5452	0.0167	0.0691	0.0008	487	77	442	11	431	5
#7-25	22.73	58.2	101	0.58	0.0733	0.0027	1.8182	0.0752	0.1760	0.0034	1033	75	1052	27	1045	19

Appendix E

Table A2. Fission-track results analysed in this study.

N _S	Area (10 ⁻⁵)	ρ _S (10 ⁵)	U (ppm)	AU (10 ⁻⁵)	1σ (U-ppm)	Date (Ma)	1σ (Ma)	D _{par} (μm)
TTL-23—rhyolite porphyry								
2	1.60	1.25	4.72	7.60	0.07	46.76	33.41	2.0
3	1.60	1.88	5.14	8.20	0.08	64.27	37.68	3.2
7	1.60	4.38	13.39	21.00	0.20	57.64	22.57	3.1
3	1.60	1.88	5.40	8.60	0.08	61.22	35.89	3.1
3	1.60	1.88	5.26	8.40	0.08	62.88	36.87	3.3
2	1.60	1.25	3.66	5.90	0.05	60.20	43.01	3.5
2	1.60	1.25	4.61	7.40	0.07	47.84	34.18	3.2
2	1.60	1.25	66.94	110.00	1.00	3.31	2.36	2.8
3	1.60	1.88	4.80	7.70	0.07	68.80	40.34	3.0
4	1.60	2.50	5.00	8.00	0.07	88.04	44.92	3.1
5	1.60	3.13	3.66	5.90	0.05	149.44	68.55	3.0
5	1.60	3.13	7.58	12.00	0.11	72.60	33.30	2.9
2	1.60	1.25	5.76	9.20	0.09	38.35	27.39	3.1
4	1.60	2.50	3.95	6.30	0.06	111.05	56.67	3.0
12	1.60	7.50	21.85	35.00	0.33	60.53	18.53	2.3
7	1.60	4.38	4.56	7.30	0.07	167.73	65.66	3.1
1	1.60	0.63	4.23	6.80	0.06	26.10	26.24	2.8
5	1.60	3.13	3.74	6.00	0.06	146.40	67.15	2.5
4	1.60	2.50	3.62	5.80	0.05	121.36	61.93	2.8
2	1.60	1.25	5.42	8.70	0.08	40.77	29.13	3.1
4	1.60	2.50	4.53	7.20	0.07	97.10	49.55	2.5
1	1.60	0.63	4.89	7.80	0.07	22.61	22.72	3.0
4	1.60	2.50	4.96	7.90	0.07	88.79	45.31	3.1
4	1.60	2.50	5.11	8.20	0.08	86.16	43.97	3.2
2	1.60	1.25	4.46	7.10	0.07	49.45	35.33	3.0
3	1.60	1.88	37.24	60.00	0.56	8.92	5.23	3.1
4	1.60	2.50	4.41	7.10	0.07	99.68	50.87	3.0
2	1.60	1.25	5.07	8.10	0.08	43.53	31.10	3.0
3	1.60	1.88	4.36	7.00	0.07	75.78	44.43	3.0
5	1.60	3.13	5.65	9.00	0.08	97.25	44.61	3.2
24	1.60	15.00	58.32	93.00	0.87	45.42	10.36	2.5
4	1.60	2.50	3.57	5.70	0.05	122.88	62.71	3.2
4	1.60	2.50	4.47	7.10	0.07	98.45	50.24	3.1
3	1.60	1.88	4.79	7.70	0.07	68.97	40.44	2.8
4	1.60	2.50	4.03	6.50	0.06	108.88	55.56	3.0
8	1.60	5.00	5.47	8.80	0.08	159.85	58.82	3.8
2	1.60	1.25	5.14	8.20	0.08	42.96	30.69	3.1
4	1.60	2.50	4.25	6.80	0.06	103.49	52.81	3.0
4	1.60	2.50	5.51	8.80	0.08	79.92	40.78	3.2
2	1.60	1.25	2.84	4.50	0.04	77.51	55.37	3.8

Table A2. *Cont.*

N _S	Area (10 ⁻⁵)	ρ_S (10 ⁵)	U (ppm)	AU (10 ⁻⁵)	1 σ (U-ppm)	Date (Ma)	1 σ (Ma)	D _{par} (μ m)
#1—fault breccia								
2	1.60	1.25	3.01	4.80	0.05	75.27	53.77	1.9
2	1.60	1.25	5.31	8.50	0.08	42.77	30.56	2.9
3	1.60	1.88	3.97	6.40	0.06	85.41	50.07	3.0
3	1.60	1.88	6.08	9.70	0.09	55.98	32.82	3.1
3	1.60	1.88	4.31	6.90	0.06	78.85	46.23	2.2
2	1.60	1.25	4.49	7.20	0.07	50.51	36.08	2.3
3	1.60	1.88	3.93	6.30	0.06	86.38	50.64	2.7
2	1.60	1.25	5.03	8.00	0.08	45.12	32.23	2.3
4	1.60	2.50	5.80	9.30	0.09	78.01	39.81	2.5
4	1.60	2.50	4.29	6.90	0.06	105.33	53.75	2.2
2	1.60	1.25	5.32	8.50	0.08	42.64	30.47	2.0
6	1.60	3.75	4.72	7.60	0.07	143.09	60.21	2.0
2	1.60	1.25	4.56	7.30	0.07	49.71	35.51	2.4
1	1.60	0.63	3.96	6.30	0.06	28.69	28.84	2.3
17	1.60	10.60	43.99	70.00	0.66	43.85	11.54	2.5
1	1.60	0.63	4.78	7.60	0.07	23.79	23.91	2.2
2	0.90	2.22	3.10	2.80	0.05	129.34	92.41	2.6
1	1.60	0.63	3.81	6.10	0.06	29.81	29.97	2.3
1	1.60	0.63	4.17	6.70	0.06	27.25	27.39	2.1
2	1.60	1.25	6.03	9.70	0.09	37.64	26.89	2.5
3	1.60	1.88	5.39	8.60	0.08	63.06	36.97	2.5
5	1.60	3.13	5.06	8.10	0.08	111.49	51.14	2.3
4	1.60	2.50	4.61	7.40	0.07	98.04	50.03	2.0
2	1.60	1.25	4.92	7.90	0.07	46.13	32.95	2.2
3	1.60	1.88	3.47	5.50	0.05	97.81	57.34	2.3
2	1.60	1.25	4.25	6.80	0.06	53.41	38.16	3.0
4	1.60	2.50	3.70	5.90	0.06	121.98	62.25	2.9
1	1.60	0.63	4.87	7.80	0.07	23.35	23.47	2.5
2	1.60	1.25	7.54	12.00	0.11	30.12	21.52	2.4
2	1.60	1.25	4.87	7.80	0.07	46.64	33.32	2.1
1	1.60	0.63	5.19	8.30	0.08	21.91	22.03	2.9
1	1.60	0.63	5.37	8.60	0.08	21.17	21.28	2.2
2	1.60	1.25	3.33	5.30	0.05	67.95	48.55	2.3
4	1.60	2.50	3.38	5.40	0.05	133.44	68.09	3.1
3	1.60	1.88	5.58	8.90	0.08	60.91	35.71	3.0
1	1.60	0.63	1.94	3.10	0.03	58.40	58.70	2.2
3	1.60	1.88	4.89	7.80	0.07	69.55	40.78	2.1

Table A2. *Cont.*

N _S	Area (10 ⁻⁵)	ρ_S (10 ⁵)	U (ppm)	AU (10 ⁻⁵)	1σ (U-ppm)	Date (Ma)	1σ (Ma)	D _{par} (μm)
#3—fault breccia								
4	1.60	2.50	7.06	11.00	0.11	62.43	31.86	2.3
4	1.60	2.50	4.95	7.90	0.07	88.83	45.33	2.8
5	1.60	3.13	4.63	7.40	0.07	118.62	54.41	2.2
4	1.60	2.50	5.93	9.50	0.09	74.32	37.93	2.2
2	1.60	1.25	13.54	22.00	0.20	16.34	11.67	2.2
5	1.60	3.13	5.05	8.10	0.08	108.68	49.85	2.6
3	1.60	1.88	5.23	8.40	0.08	63.17	37.04	2.3
3	1.60	1.88	5.86	9.40	0.09	56.45	33.10	2.1
5	1.60	3.13	5.69	9.10	0.09	96.56	44.29	2.3
3	1.60	1.88	5.63	9.00	0.08	58.76	34.45	2.1
2	1.60	1.25	4.23	6.80	0.06	52.18	37.28	2.6
3	1.60	1.88	5.38	8.60	0.08	61.50	36.06	2.1
5	1.60	3.13	4.27	6.80	0.06	128.52	58.95	2.2
4	1.60	2.50	4.54	7.30	0.07	96.86	49.43	2.6
2	1.60	1.25	5.76	9.20	0.09	38.31	27.37	2.8
1	1.60	0.63	4.54	7.30	0.07	24.37	24.50	2.2
5	1.60	3.13	5.84	9.40	0.09	94.07	43.15	2.9
2	1.60	1.25	5.06	8.10	0.08	43.66	31.19	3.0
3	1.60	1.88	4.64	7.40	0.07	71.19	41.74	2.2
5	1.60	3.13	3.99	6.40	0.06	137.35	63.00	2.3
2	1.60	1.25	5.00	8.00	0.07	44.19	31.57	2.1
4	1.60	2.50	7.31	12.00	0.11	60.32	30.78	2.3
1	1.60	0.63	2.39	3.80	0.04	46.24	46.48	2.0
5	1.60	3.13	5.03	8.00	0.08	109.16	50.07	3.0
4	1.60	2.50	5.13	8.20	0.08	85.84	43.80	2.2
2	1.60	1.25	4.85	7.80	0.07	45.52	32.52	2.9
1	1.60	0.63	5.65	9.00	0.08	19.56	19.67	2.5
4	1.60	2.50	6.12	9.80	0.09	71.96	36.72	2.2
2	1.60	1.25	4.16	6.70	0.06	53.06	37.91	2.0
2	1.60	1.25	4.54	7.30	0.07	48.62	34.73	2.1
3	1.60	1.88	12.77	20.00	0.19	25.96	15.22	2.1
3	1.60	1.88	5.40	8.60	0.08	61.22	35.89	2.3
3	1.60	1.88	8.02	13.00	0.12	41.32	24.22	2.1
3	1.60	1.88	6.98	11.00	0.10	47.42	27.80	2.1
2	1.60	1.25	5.41	8.70	0.08	40.79	29.14	3.0
3	1.60	1.88	3.67	5.90	0.06	89.91	52.71	3.1
2	1.60	1.25	5.86	9.40	0.09	37.71	26.94	2.3
3	1.60	1.88	6.08	9.70	0.09	54.44	31.92	2.8
4	1.60	2.50	5.74	9.20	0.09	76.66	39.12	2.3
4	1.60	2.50	4.07	6.50	0.06	108.03	55.12	2.6

Table A2. *Cont.*

N _S	Area (10 ⁻⁵)	ρ_S (10 ⁵)	U (ppm)	AU (10 ⁻⁵)	1 σ (U-ppm)	Date (Ma)	1 σ (Ma)	D _{par} (μ m)
MKZ2-A90—fault breccia								
2	1.60	1.25	3.10	5.00	0.05	73.16	52.27	2.0
3	1.60	1.88	4.47	7.10	0.07	76.05	44.59	2.0
3	1.60	1.88	4.83	7.70	0.07	70.42	41.28	2.1
3	1.60	1.88	3.85	6.20	0.06	88.11	51.66	2.2
5	1.60	3.13	6.40	10.00	0.10	88.41	40.56	2.2
3	1.60	1.88	5.22	8.30	0.08	65.14	38.19	2.3
8	1.60	5.00	4.44	7.10	0.07	201.95	74.31	2.0
3	1.60	1.88	4.16	6.70	0.06	81.59	47.84	2.8
3	1.60	1.88	4.33	6.90	0.06	78.49	46.02	2.1
4	1.60	2.50	3.99	6.40	0.06	113.21	57.77	2.1
4	1.60	2.50	5.02	8.00	0.08	90.05	45.95	2.1
3	1.60	1.88	4.96	7.90	0.07	68.55	40.19	2.2
2	1.60	1.25	4.08	6.50	0.06	55.55	39.69	2.0
4	1.60	2.50	5.86	9.40	0.09	77.23	39.41	2.1
2	1.60	1.25	4.61	7.40	0.07	49.17	35.13	2.1
2	1.60	1.25	4.64	7.40	0.07	48.91	34.94	1.9
2	1.60	1.25	5.23	8.40	0.08	43.42	31.02	2.2
3	1.60	1.88	4.68	7.50	0.07	72.52	42.52	2.4
7	1.60	4.38	26.19	42.00	0.39	30.36	11.89	2.1
3	1.60	1.88	4.95	7.90	0.07	68.65	40.25	2.2
2	1.60	1.25	4.03	6.50	0.06	56.21	40.15	2.1
2	1.60	1.25	5.62	9.00	0.08	40.39	28.86	2.0
3	1.60	1.88	5.22	8.40	0.08	65.11	38.17	2.4
6	1.60	3.75	3.52	5.60	0.05	191.42	80.55	2.2
4	1.60	2.50	5.02	8.00	0.08	90.11	45.98	2.2
3	1.60	1.88	4.65	7.40	0.07	73.00	42.80	2.1
2	1.60	1.25	4.53	7.20	0.07	50.13	35.81	2.1
2	1.60	1.25	5.12	8.20	0.08	44.29	31.64	2.1
9	1.60	5.63	4.78	7.60	0.07	211.04	73.57	2.5
4	1.60	2.50	5.17	8.30	0.08	87.56	44.68	2.3
4	1.60	2.50	5.96	9.50	0.09	75.92	38.74	2.2
4	1.60	2.50	4.84	7.80	0.07	93.34	47.63	2.1
3	1.60	1.88	4.91	7.80	0.07	69.26	40.61	2.2
4	1.60	2.50	4.76	7.60	0.07	95.04	48.50	2.1
5	1.60	3.13	4.96	7.90	0.07	113.77	52.19	2.0
5	1.60	3.13	5.42	8.70	0.08	104.20	47.80	2.4
6	1.60	3.75	2.49	4.00	0.04	268.39	112.94	2.5
3	1.60	1.88	5.34	8.50	0.08	63.66	37.32	2.1
2	1.60	1.25	4.47	7.10	0.07	50.77	36.27	2.1
3	1.60	1.88	4.55	7.30	0.07	74.72	43.81	2.6

Note: All the errors are 1 σ . N_S: the number of spontaneous fission tracks; area: the area of spots; ρ_S : the density of spontaneous fission tracks; U: U content; AU: area \times U; date: the fission-track date of the grain; D_{par}: the mean D_{par} value of the grain. The methodology applied was based on direct U determination using an LA-ICP-MS [32,33]. Each grain used to determine the spontaneous fission-track density was characterized using an LA-ICP-MS and the data normalization was carried out using the $^{43}\text{Ca}/^{238}\text{U}$ of the standard sample (std) and an unknown sample (unk) based on the following correlation: $[U]_{\text{unk}} = \{[({}^{43}\text{Ca}/{}^{238}\text{U})_{\text{unk}}]/[({}^{43}\text{Ca}/{}^{238}\text{U})_{\text{std}}]\} \times (U_{\text{std}})$ [32,33].

References

1. Foster, D.A.; Ehlers, K. $^{40}\text{Ar}/^{39}\text{Ar}$ thermochronology of the southern Gawler craton, Australia: Implications for Mesoproterozoic and Neoproterozoic tectonics of east Gondwana and Rodinia. *J. Geophys. Res.* **1998**, *103*, 10177–10193. [[CrossRef](#)]
2. Dezes, D.J.; Vannay, J.C.; Steck, A.; Bussy, F.; Cosca, M. Synorogenic extension: Quantitative constraints on the age and displacement of the Zanskar shear zone (northern Himalaya). *Geol. Soc. Am. Bull.* **1999**, *111*, 364–374. [[CrossRef](#)]
3. Lee, H.; Yang, J. ESR dating of the Eupchon fault, South Korea. *Quat. Geochronol.* **2007**, *2*, 392–397. [[CrossRef](#)]
4. Hu, L.; He, D.F.; Hu, D.G. Electron Spin Resonance Dating of the Late Cenozoic Deformation of the Huoerguosi-Manas-Tugulu Reverse Faults along Southern Edge of Junggar Basin. *Acta Geosci. Sin.* **2005**, *2*, 121–126. (In Chinese with English Abstract)

5. Wang, X.M.; Zhong, D.L.; Zhang, J.J.; Ji, J.Q.; Wang, X.S. Low-Temperature Thermochronological Constraints on Sinistral Strike-Slip Movement of the Yi-Shu Fault Zone between the Late Cretaceous and Early Paleogene. *Acta Geol. Sin.* **2007**, *81*, 454–465. (In Chinese with English Abstract)
6. Zhu, Y.L.; Liang, Z.R.; Shi, R.J. The Determination of Age of the Fault Activities of Shougou Hill, Guangzhou by Thermoluminescence Dating and Nuclear Fission Track Dating. *Acta Sci. Nat. Univ. Sunyatseni* **1996**, *35*, 54–58. (In Chinese with English Abstract)
7. Zhang, F.; Lin, W.; Zhou, J. The age of Xiannü Mountain fracture belt in Three-Gorge region. *Chin. Sci. Bull.* **1999**, *44*, 744–747. [[CrossRef](#)]
8. Wölfler, A.; Kurz, W.; Danišík, M.; Rabitsch, R. Dating of fault zone activity by apatite fission track and apatite (U-Th)/He thermochronometry: A case study from the Lavanttal fault system (Eastern Alps). *Terra Nova* **2010**, *22*, 274–282.
9. Tagami, T. Application of Fission-Track Thermochronology to Understand Fault Zones. In *Fission-Track Thermochronology and its Application to Geology*; Malusà, M.G., Fitzgerald, P.G., Eds.; Springer International Publishing: Cham, Switzerland, 2019; pp. 221–233.
10. Xiang, H.F.; Wan, J.L.; Han, Z.J.; Guo, S.M.; Zhang, W.X.; Chen, L.C.; Dong, X.Q. Geological analysis and FT dating of the large-scale right-lateral strike-slip movement of the Red River fault zone. *Sci. China Ser D-Earth Sci.* **2007**, *50*, 331–342. [[CrossRef](#)]
11. Ito, H. Apatite fission-track dating of fault-related rocks along the Nojima and Kusumoto faults and its tectonic significance. *Geophys. Res. Lett.* **2004**, *31*, 1–4. [[CrossRef](#)]
12. Zhang, B.L.; Liu, R.X.; Xiang, H.F.; Wan, J.L.; Huang, X.N. FT dating of fault rocks in the central-southern section of the red river fault zone and its geological implications. *Seismol. Geol.* **2009**, *31*, 44–56. (In Chinese with English Abstract)
13. Warren-Smith, E.; Lamb, S.; Seward, D.; Smith, E.; Herman, F.; Stern, T. Thermochronological evidence of a low-angle, mid-crustal detachment plane beneath the central South Island, New Zealand. *Geochem. Geophys. Geosystems* **2016**, *17*, 4212–4235. [[CrossRef](#)]
14. Yamada, R.; Matsuda, T.; Omura, K. Apatite and zircon fission-track dating from the Hirabayashi-NIED borehole, Nojima Fault, Japan: Evidence for anomalous heating in fracture zones. *Tectonophysics* **2007**, *443*, 153–160. [[CrossRef](#)]
15. d’Alessio, M.A.; Blythe, A.E.; Bürgman, R. No frictional heat along the San Gabriel fault, California: Evidence from fission-track thermochronology. *Geology* **2003**, *31*, 541–544. [[CrossRef](#)]
16. Guangdong Geological Bureau. *Regional Geological Record of Guangdong Province*; Geology Press: Beijing, China, 1988.
17. Ren, D.J.; Shen, S.L.; Cheng, W.C.; Zhang, N.; Wang, Z.F. Geological formation and geo-hazards during subway construction in Guangzhou. *Environ. Earth Sci.* **2016**, *75*, 1–14. [[CrossRef](#)]
18. Ren, Z.H.; Ye, X.W.; Huang, J.T.; Liao, G.J.; Sun, C.C.; Liu, T.Y.; Qiao, J.H.; Wei, W. Deep faults interpreted by gravity-magnetic data in the pearl river delta region and their neotectonic significance. *Quat. Sci.* **2009**, *29*, 625–632. (In Chinese with English Abstract)
19. Bi, L.S.; Huang, J.T.; Ren, Z.H.; Ye, X.W.; Lu, B.H.; Liu, T.Y.; Qiao, J.H. Deep faults in the Pearl River Delta region based on aeromagnetic data interpretation. *Acta Sci. Nat. Univ. Sunyatseni* **2021**, *60*, 90–99. (In Chinese with English Abstract)
20. Zou, H.P.; Qiu, Y.X.; Zhuang, W.M.; Shao, R.S. Determination of deformation stages of the Shougouling fault zone in the Guangzhou area. *Reg. Geol. China* **2001**, *1*, 67–81. (In Chinese with English Abstract)
21. Guo, Q.H.; Guo, L.T.; Chen, P.L. Assessment of Urban Seismogeologic Disasters in Guangzhou City. *S. China J. Seismol.* **2008**, *2*, 85–94. (In Chinese with English Abstract)
22. Li, J.R.; Wu, Q.S.; Liu, S. Study on the Characteristics of Fault and Suggestion of Engineering Measures at Jiangtai Road Station of Guangzhou Metro Extend Two & Eight. *Guangzhou Archit.* **2006**, *6*, 28–32. (In Chinese with English Abstract)
23. Pan, J.X. Seismogenic structure in Guangzhou area and its seismic risk. *S. China J. Seismol.* **1992**, *12*, 32–41. (In Chinese with English Abstract)
24. Yan, P.; Liu, H.L. Temporal and spatial distributions of meso-cenozoic igneous rocks over south China sea. *J. Trop. Oceanogr.* **2005**, *2*, 33–41. (In Chinese with English Abstract)
25. Lin, B.H.; Yang, S.Z.; Zhu, B.S.; Wu, H.X. Geological structure and basic geotechnical characteristics in guangdong province. *Chin. J. Rock Mech. Eng.* **2006**, *25*, 3337–3346. (In Chinese with English Abstract)
26. Hou, W.S.; Chen, X.W.; Yang, Q.C.; Chen, Y.H. The uncertainty analysis of 3D fault zone model and its application in metro engineering. *Acta Sci. Nat. Univ. Sunyatseni* **2021**, *60*, 58–67. (In Chinese with English Abstract)
27. Dong, H.G. *Activity and Tectonic Evolution of Major North-West Trending Faults in the Pearl River Delta*; China University of Geosciences Press: Wuhan, China, 2015.
28. Hou, M.C.; Chen, H.D.; Li, Z.Z.; Wan, L.; Li, G.X. Study on the Depositional system of the Sanshui basin, Guangdong, China. *Geol. Bull. China* **2006**, *25*, 1175–1183. (In Chinese with English Abstract)
29. Chen, P.P. The Response of Late Cretaceous-Eocene Epoch Volcanic and Sedimentary Sequence in Sanshui Basin to the Tectonic Evolution of the Northern Margin of South China Sea. Ph.D. Thesis, China University of Geosciences, Beijing, China, 2018; p. 118. (In Chinese with English Abstract)
30. Liu, Y.S.; Hu, Z.C.; Zong, K.Q.; Gao, C.G.; Gao, S.; Xu, J.; Chen, H.H. Reappraisal and refinement of zircon U-Pb isotope and trace element analyses by LA-ICP-MS. *Chin. Sci. Bull.* **2010**, *55*, 1535–1546. [[CrossRef](#)]
31. Ludwig, K.R. *ISOPLOT 3.0: A Geochronological Toolkit for Microsoft Excel*; Berkeley Geochronology Center Special Publication: Berkeley, CA, USA, 2003.

32. Soares, C.J.; Guedes, S.; Hadler, J.C.; Mertz-Kraus, R.; Zack, T.; Iunes, P.J. Novel calibration for LA-ICP-MS based fission-track thermochronology. *Phys. Chem. Min.* **2014**, *41*, 65–73. [[CrossRef](#)]
33. Soares, C.J.; Mertz-Klaus, R.; Guedes, S.; Stockli, D.F.; Zack, T. Characterization of apatites as potential trace element reference materials for fission-track dating by LA-ICP-MS. *Geostand. Geoanalytical Res.* **2014**, *39*, 305–313. [[CrossRef](#)]
34. Ding, R.X. Low temperature thermal history reconstruction based on apatite fission-track length distribution and apatite U-Th/He age using Low-T Thermo. *J. Earth Sci. China* **2020**, *1*–24.
35. Vermeesch, P. Radial Plotter: A Java application for fission track, luminescence and other radial plots. *Radiat. Meas.* **2009**, *44*, 409–410. [[CrossRef](#)]
36. Ketcham, R.A.; Carter, A.; Donelick, R.A.; Barbarand, J.; Hurford, A.J. Improved modeling of fission-track annealing in apatite. *Am. Miner.* **2007**, *92*, 799–810. [[CrossRef](#)]
37. Li, X.M.; Zou, H.P. Late Cretaceous-Cenozoic exhumation of the southeastern margin of Coastal Mountains, SE China, revealed by fission-track thermochronology: Implications for the topographic evolution. *Solid Earth Sci.* **2017**, *2*, 79–88. [[CrossRef](#)]
38. Tang, D.L.K.; Seward, D.; Wilson, C.J.N.; Sewell, R.J.; Carter, A.; Paul, B.T. Thermotectonic history of SE China since the Late Mesozoic: Insights from detailed thermochronological studies of Hong Kong. *J. Geol. Soc.* **2014**, *171*, 591–604. [[CrossRef](#)]
39. Ding, R.X.; Min, K.; Zou, H.P. Inversion of topographic evolution using low-T thermal history: A case study from coastal mountain system in Southeastern China. *Gondwana Res.* **2019**, *67*, 21–32. [[CrossRef](#)]